



1 Modeling Regional Air Quality and Climate: Improving Organic Aerosol and Aerosol Activation  
2 Processes in WRF/Chem version 3.7.1  
3

4 Khairunnisa Yahya<sup>1</sup>, Timothy Glotfelty<sup>1</sup>, Kai Wang<sup>1</sup>, Yang Zhang<sup>1\*</sup>, and Athanasios Nenes<sup>2,3,4,5</sup>

5 <sup>1</sup>Department of Marine, Earth, and Atmospheric Sciences, North Carolina State University,  
6 Raleigh, North Carolina, U.S.A.

7 <sup>2</sup>School of Earth and Atmospheric Sciences, Georgia Institute of Technology, Atlanta, GA,  
8 U.S.A

9 <sup>3</sup>School of Chemical and Biomolecular Engineering, Georgia Institute of Technology, Atlanta,  
10 GA, U.S.A.

11 <sup>4</sup>Institute of Environmental Research & Sustainable Development, National Observatory of  
12 Athens, Greece

13 <sup>5</sup>Institute for Chemical Engineering Science, Foundation for Research and Technology-Hellas,  
14 Patra, Greece

15

16 Email: \*yang\_zhang@ncsu.edu

17

## ABSTRACT

18 Air quality and climate influence each other through the uncertain processes of aerosol formation  
19 and cloud droplet activation. In this study, both processes are improved in the Weather, Research  
20 and Forecasting model with Chemistry (WRF/Chem) version 3.7.1. The existing Volatility Basis  
21 Set (VBS) treatments for organic aerosol (OA) formation in WRF/Chem is improved by  
22 considering the secondary OA (SOA) formation from semi-volatile primary organic aerosol  
23 (POA), a semi-empirical formulation for the enthalpy of vaporization of SOA, as well as  
24 functionalization and fragmentation reactions for multiple generations of products from the  
25 oxidation of VOCs. Two-month long simulations (May to June 2010) are conducted over  
26 continental U.S. and results are evaluated against surface and aircraft observations during the  
27 Nexus of Air Quality and Climate Change (CalNex) campaign. Among all the configurations  
28 considered, the best performance is found for the simulation with the 2005 Carbon Bond  
29 mechanism (CB05) and the VBS SOA module with semivolatile POA treatment, 25%



30 fragmentation, and the emissions of semi-volatile and intermediate volatile organic compounds  
31 being 3 times of the original POA emissions. Among the three gas-phase mechanisms (CB05,  
32 CB6, and SAPRC07) used, CB05 gives the best performance for surface ozone and PM<sub>2.5</sub>  
33 concentrations. Differences in SOA predictions are larger for the simulations with different VBS  
34 treatments (e.g., non-volatile POA vs. semivolatile POA) as compared to the simulations with  
35 different gas-phase mechanisms. Compared to the simulation with CB05 and the default SOA  
36 module, the simulations with the VBS treatment improve cloud droplet number concentration  
37 (CDNC) predictions (NMBs from -40.8% to a range of -34.6% to -27.7%), with large differences  
38 between CB05/CB6 and SAPRC07 due to large differences in their OH and HO<sub>2</sub> predictions. An  
39 advanced aerosol activation parameterization based on the FN05 series reduces the large negative  
40 CDNC bias associated with the default ARG00 parameterization from -35.4% to a range of -0.8%  
41 to 7.1%, it, however, increases the errors due to overpredictions of CDNC, mainly over  
42 northeastern U.S. This work indicates a need to improve other aerosol-cloud-radiation processes  
43 in the model such as the spatial distribution of aerosol optical depth and cloud condensation nuclei  
44 in order to further improve CDNC predictions.

## 45 **1. Introduction**

46

47 The Intergovernmental Panel on Climate Change (IPCC) report on the AR5 scenario attributes  
48 the aerosol radiative forcing (RF) to be the dominant source of uncertainty contributing to the  
49 overall uncertainty in the net Industrial Era Radiative Forcing (RF) calculations (Myhre et al.,  
50 2013). Despite the inclusion of more aerosol processes in the current generation of atmospheric  
51 models, differences between atmospheric models and observations continue to persist. Aerosols  
52 affect the climate through the direct effect by absorbing or scattering radiation, or the indirect  
53 effect by acting as cloud condensation nuclei (CCN). According to Hallquist et al. (2009), the



54 formation of inorganic particulates such as sulfate, nitrate, and ammonium are well understood,  
55 however, there are large uncertainties in the formation of secondary organic aerosol (SOA). As a  
56 result, current models do not have a comprehensive treatment of OA, which usually result in an  
57 underprediction of OA concentrations (Hodzic et al., 2010; Jathar et al., 2011; Bergstrom et al.,  
58 2012), due to missing key precursors and processes in OA formation (Ahmadov et al., 2012). Some  
59 of the missing key precursors in most models include semi-volatile primary organic aerosol (POA),  
60 long-chain *n*-alkanes, polycyclic aromatic hydrocarbons (PAHs), and large olefins that have lower  
61 volatilities compared to traditional SOA precursors (Chan et al., 2009). The organic carbon (OC)  
62 component of the radiative forcing in the IPCC AR5 report also does not include SOA with the  
63 reason that the formation is dependent on a number of factors that are not currently sufficiently  
64 quantified (Myhre et al., 2013). However, SOA can form a significant percentage of total OA (up  
65 to 95% in rural areas) (Zhang et al., 2007). Another large source of uncertainty is the quantification  
66 of clouds as well as aerosol-cloud interactions due to incomplete or inaccurate representations of  
67 these processes in climate models (Boucher et al., 2013). A major process in cloud formation from  
68 aerosol is aerosol activation, which involves the condensational growth of aerosols in a cooling air  
69 parcel until maximum supersaturation, and some of the wet particles reach a critical radius where  
70 they are then able to grow spontaneously into cloud droplets (Ghan et al., 2011). Various  
71 approaches have been developed to reduce the uncertainties associated with OA and aerosol  
72 activation treatments in climate models. Those treatments are reviewed in the following section.

### 73 **1.1. VBS Treatments and Sensitivity to Different Gas-Phase Chemical Mechanisms in** 74 **Regional and Global Models**

75  
76 Unlike inorganic aerosols such as sulfate, the physical and chemical properties of OA  
77 dynamically evolve with age (Jimenez et al., 2009). The traditional approach to modeling SOA is



78 to assume that each VOC precursor forms several surrogate compounds (Odum et al., 1996).  
79 However, the traditional method has several shortcomings, for example, two products are needed  
80 for each VOC precursor causing this method to be computationally-expensive if many VOC  
81 precursors are treated in the model (Murphy and Pandis, 2009). The assumption that the products  
82 are unreactive also does not reflect the dynamic nature of the first generation products from the  
83 oxidation of VOCs that can undergo successive oxidation steps to further produce lower volatility  
84 products (Jimenez et al., 2009). The volatility basis set (VBS) is a framework developed by  
85 Donahue et al. (2006), which is able to simulate gas-phase partitioning and multiple generations  
86 of gas-phase oxidation of organic vapors. This approach addresses the shortcomings of the  
87 traditional SOA modeling approach as it can cover the complete volatility range of OA compounds  
88 (Murphy and Pandis, 2009).

89 Table 1 summarizes some of the VBS treatments from current regional and global models. The  
90 VBS treatment has been implemented into a number of regional models such as the Weather,  
91 Research and Forecasting model with Chemistry (WRF/Chem) (Shrivastava et al., 2011;  
92 Ahmadov et al., 2012), the Particulate Matter Comprehensive Air Quality Model with extensions  
93 (PMCAMx) (Lane et al., 2008; Donahue et al., 2009; Murphy et al., 2009), and CHIMERE (Hodzic  
94 et al., 2010). It has also been implemented in global models such as GISS II' GCM (Farina et al.,  
95 2010; Jathar et al., 2011) and the Community Earth System Model (CESM) (Shrivastava et al.,  
96 2015). Different studies define the classifications of the organic species slightly differently.  
97 Donahue et al. (2009) defined primary organic vapors with effective saturation concentrations ( $C^*$ )  
98 of  $10^{-2}$  -  $10^{-1}$ ,  $10^0$  -  $10^2$ , and  $10^3$  -  $10^6$   $\mu\text{g m}^{-3}$  at 298 K to be low volatility organic compounds  
99 (LVOCs), semi-volatile organic compounds (SVOCs), and intermediate volatility organic  
100 compounds (IVOCs), respectively. Shrivastava et al., (2011) and Jathar et al. (2011) defined





101 primary organic vapors with  $C^*$  values of  $10^{-2}$  -  $10^3$  and  $10^4$  -  $10^6$   $\mu\text{g m}^{-3}$  to be SVOCs and IVOCs,  
102 respectively. All those studies defined VOCs to be gas-phase organic species with  $C^*$  larger than  
103  $10^6$   $\mu\text{g m}^{-3}$  at 298 K.

104 The traditional emission inventories used in the chemical transport models consist of VOCs  
105 but not SVOCs or IVOCs as both SVOCs and IVOCs are difficult to measure. This is most likely  
106 because SVOCs and IVOCs tend to evaporate at high temperatures from combustion sources  
107 (Donahue et al., 2009). As the traditional SOA approach usually underpredicts the SOA  
108 concentration, the addition of the SVOC and IVOC emissions on top of the existing VOC  
109 emissions in most emission inventories can improve model performance. To account for the  
110 missing key precursors in OA formation, SVOC and IVOC emissions are usually estimated as a  
111 factor of existing POA emissions in current emission inventories. For example, Shrivastava et al.  
112 (2011) estimated the sum of all SVOC and IVOC precursors to be 7.5 times the mass of traditional  
113 POA emissions inventory over Mexico City, but indicated that the scaling factor of 3 for SVOC  
114 emissions based on the POA emissions is poorly constrained. Shrivastava et al. (2008) and Jathar  
115 et al. (2011) assumed that SVOC emissions are represented by the traditional emission inventory  
116 while IVOC emissions are 1.5 times the traditional emission inventory. Pye and Seinfeld (2010)  
117 assumed that SVOC emissions are a subset of traditional POA emission inventories, and their POA  
118 emissions were scaled up by 27% on a global scale. IVOC emissions are assumed to be spatially-  
119 distributed similar to naphthalene and are predicted to be roughly a factor of half of global POA  
120 emissions. Tsimpidi et al. (2014) assumed that the IVOC emissions are 1.5 times the traditional  
121 POA emission inventory and are assigned to the 4<sup>th</sup> volatility bin with  $C^* = 10^5$   $\mu\text{g m}^{-3}$ . For  
122 comparison, some studies such as Ahmadov et al. (2012) and Bergstrom et al. (2012) used the  
123 VBS approach for OA modeling but did not include additional SVOC emissions. There are also



124 differences in the volatility distribution used in literature. Shrivastava et al. (2008) and Jathar et  
125 al. (2011) found that moving half the mass of SVOC from all bins to the lowest bin from the  
126 traditional “diesel exhaust” volatility distribution of Robinson et al. (2007) produced the lowest  
127 errors in simulated OA on an annual average basis.

128 The number of bins used can also result in differences in simulated SOA concentrations.  
129 Shrivastava et al. (2011) showed that the 2-species VBS performed better than the 9-species VBS  
130 in modeling oxygenated organic aerosol (OOA) and gave the closest agreement to the OOA  
131 calculated by the Positive Matrix Factorization (PMF) method. This indicates that SOA may be  
132 less volatile as compared to the volatility distribution in the 9-species VBS which allows for  
133 evaporation of SOA with dilution (Shrivastava et al., 2011).

134 The amount of oxygen added for each oxidation step may contain uncertainties. This factor  
135 can influence the O:C ratio used for the model evaluation. O:C predictions from models need to  
136 be improved by including fragmentation reactions (which could lead to an increase in O:C ratios)  
137 and improving emission estimates (Shrivastava et al., 2011). Different rate constants can also result  
138 in different predictions of SOA concentrations. For example, Farina et al. (2010) showed that the  
139 use of k value of  $1 \times 10^{-12} \text{ cm}^3 \text{ molecule}^{-1} \text{ s}^{-1}$  compared to the default k value of  $10 \times 10^{-12} \text{ cm}^3$   
140  $\text{molecule}^{-1} \text{ s}^{-1}$  resulted in a reduced aged SOA formation by 71%. Hodzic et al. (2010) also showed  
141 a case study based on Grieshop et al. (2009) in which each oxidation step reduced the volatility of  
142 the S/IVOC vapors by two orders of magnitude and each successive oxidation step produced a  
143 40% increase in mass due to the addition of oxygen. This case is inconclusive in urban areas - a  
144 larger bias along with a higher correlation coefficient compared to the more common case where  
145 each oxidation step reduced the volatility by one order of magnitude with a 7.5% increase in mass.



146 However, the model performed worse (with larger bias and lower correlation coefficient) in  
147 suburban areas.

148 The aging process improves model performance in general in the United States (U.S.) but  
149 deteriorates the performance in several parts of Europe. Accounting for the aging process of OA  
150 will increase the OA concentrations and improve model results in the U.S. where OA is usually  
151 underpredicted, but increase the model bias for OA in several parts of Europe where OA  
152 concentrations are overpredicted (Farina et al., 2010; Bergstrom et al., 2012).

153 Shrivastava et al. (2013) studied the effects of the fragmentation and functionalization in VBS.  
154 Functionalization increases the mass of OA for each successive oxidation step, while  
155 fragmentation reduces the mass for each oxidation step. One such a case includes simulating first-  
156 order effects of the fragmentation and functionalization processes in VBS by assuming  
157 functionalization of 100% of organic vapors for the first two generations of oxidation and both  
158 fragmentation and functionalization for the third and higher generations of oxidation. The  
159 fragmentation reduces the SOA concentrations drastically. For example, Shrivastava et al. (2013)  
160 showed that peak SOA concentrations can be reduced by factors of 2 to 4 for a 1-hour example on  
161 10 March 2006 at 21 UTC over Mexico City Plateau.

162 The VBS framework for OA modeling in the latest version of WRF/Chem, v3.7.1, is coupled  
163 with several gas-phase mechanisms including the 2005 Carbon Bond Mechanism (CB05)  
164 (Yarwood et al., 2005), the Model for Ozone and Related chemical Tracers version 4 (MOZART-  
165 4) (Emmons et al., 2010), the Regional Atmospheric Chemistry Model (RACM) (Stockwell et al.,  
166 1997), and the 1999 version of the Statewide Air Pollution Research Centre (SAPRC99)  
167 mechanism (Carter, 2000). Different gas-phase mechanisms have different lumpings/groupings  
168 for VOCs, which will affect OA formation. For example, VOCs are lumped according to their



169 carbon bonds (e.g., single or double bond) in CB05 (Yarwood et al., 2005) while VOCs in  
170 SAPRC99 (Carter, 2000) are lumped according to their OH reactivities. A number of studies  
171 examined the differences in predicting O<sub>3</sub> concentrations due to different gas-phase mechanisms  
172 (e.g., Luecken et al., 2008; Li et al., 2012; Shearer et al., 2012; Zhang et al., 2012), but fewer  
173 studies reported the impact of different gas-phase mechanisms on modeling SOA and PM<sub>2.5</sub>  
174 concentrations (Kim et al., 2011; Zhang et al., 2012). SAPRC99 has more detailed organic  
175 chemistry compared to CB05. SAPRC99 has been updated to SAPRC07 (and recently, to  
176 SAPRC11) based on newly available information regarding the reactions and influence of  
177 individual VOCs on O<sub>3</sub>, as well as evaluations against chamber experiments (Carter, 2010). In  
178 addition, SAPRC07 has reformulated reactions of peroxy radicals so that the effects of changes in  
179 nitrogen oxides (NO<sub>x</sub>) on organic product formation is more accurately represented. SAPRC07  
180 has the most extensive set of VOC species and reactions, as compared to CB05 and the Carbon  
181 Bond version 6 (CB6). Shearer et al. (2012) reported that a condensed version of SAPRC07  
182 predicted lower O<sub>3</sub> and OH concentrations in central California compared to SAPRC99 due to a  
183 decreased reaction rate coefficient in the reaction of OH and NO<sub>2</sub> to form HNO<sub>3</sub>. Li et al. (2012)  
184 also showed that predicted O<sub>3</sub> concentrations from SAPRC07 were lower than those of SAPRC99  
185 by up to 20% over Texas. The same study also reported that SAPRC07 gave lower OH  
186 concentrations due to differences in the reaction rate constants in the reactions of O<sup>1</sup>D and H<sub>2</sub>O  
187 between SAPRC07 and SAPRC99. Luecken et al. (2008) reported that SAPRC99 gave higher O<sub>3</sub>  
188 concentrations compared to CB05 on average; however, the differences vary with locations,  
189 VOC/NO<sub>x</sub> ratios, and the concentrations of precursor pollutants. This is consistent with the results  
190 from Zhang et al. (2012), which predicted that SAPRC99 using WRF/Chem with the Model of  
191 Aerosol, Dynamics, Reaction, Ionization and Dissolution (WRF/Chem-MADRID) produced the



192 highest O<sub>3</sub> mixing ratios in July at the Southeastern Aerosol Research and Characterization  
193 (SEARCH) sites. The CB6 (Yarwood et al., 2010) is an updated version of CB05 with improved  
194 kinetic and photolysis data, additional explicit species for long-lived and abundant organic  
195 compounds including propane, acetone, benzene and acetylene, as well as revised isoprene and  
196 aromatics chemistry from CB05. Yarwood et al. (2010) showed that CB6 produces higher daily  
197 maximum 8-hr O<sub>3</sub> as compared to CB05 over Los Angeles for one episode day in August with the  
198 highest observed O<sub>3</sub> mixing ratios. CB6 was also shown to produce substantially higher OH  
199 concentrations (25% to 50% higher at mid-day over large areas) over eastern U.S. compared to  
200 CB05 over a few days in June, 2006. A summary of the main characteristics of CB05, CB6, and  
201 SAPRC07 gas-phase mechanisms are listed in Table 2.

## 202 1.2. Description of Aerosol Activation Parameterizations

203

204 Ghan et al. (2011) provided a comprehensive review on various aerosol activation treatments  
205 in current climate models. Two main types of parameterizations are commonly used: the Abdul-  
206 Razzak and Ghan (2000) (AR-G00) and the Fountoukis and Nenes (2005) (FN05) and associated  
207 updates described in Barahona et al. (2010) and Morales Betancourt and Nenes (2014). AR-G00  
208 uses multiple lognormal or sectional distributions to approximate the aerosol size distribution. It  
209 uses the Kohler theory to relate the aerosol size distribution and composition to the number of  
210 aerosols activated as a function of maximum supersaturation ( $S_{\max}$ ). The complex function  
211 involving  $S_{\max}$  is parameterized based on the standard deviation  $\sigma$  from a large number of  
212 numerical solutions using a cloud parcel model. The number and mass activated are particles with  
213 critical supersaturation less than  $S_{\max}$ . It also accounts for particle growth before and after the  
214 particles are activated. However, the ARG treatment does not explicitly represent kinetic  
215 limitations which tend to affect smaller or larger particles (with diameters far from their critical



216 size). Very small particles tend to lose water when supersaturation declines as they never exceed  
217 the critical supersaturation for that particle size, and very large particles may not have achieved  
218 the critical size before  $S_{\max}$  is reached (Ghan et al., 2011). Kinetic limitations refer to the (i) inertial  
219 mechanism – where particles with large dry diameters grow to be as large as activated particles  
220 but have not been activated themselves, these particles should be considered together with  
221 activated particles; (ii) evaporation mechanism – where particles with high critical supersaturation  
222 evaporate before reaching their critical diameters; and the (iii) deactivation mechanism – where  
223 initially activated particles that are deactivated to interstitial aerosols when the parcel  
224 supersaturation falls below the equilibrium supersaturation (Nenes et al., 2001). Neglecting kinetic  
225 limitations performs well for all conditions except in highly-polluted areas (Ghan et al., 2011). In  
226 urban and highly-polluted cases, many particles fail to be activated due to strong evaporation and  
227 deactivation processes (Nenes et al., 2001). Explicitly accounting for kinetic limitations reduces  
228 CDNC at low updraft velocity (Ghan et al., 2011).

229       The Fountoukis and Nenes (2005) (FN05) scheme improved the ARG00 scheme by solving  
230  $S_{\max}$  analytically (with the exception of kinetically-limited particles) using a so-called “population  
231 splitting” method. In addition, FN05 took into account the kinetic limitations, as well as the  
232 influence of gas kinetics on water vapor diffusivity (Ghan et al., 2011). The other improved  
233 treatments built on top of the FN05 scheme include the entrainment of ambient air, which could  
234 reduce the supersaturation of the updraft (Barahona and Nenes, 2007) (BN07) (therefore reducing  
235 CDNC); the adsorption of water vapor onto insoluble particles by Kumar et al. (2009) (KU09)  
236 based on a modified Frenkel-Halsey-Hill (FHH) adsorption theorem (which will increase CDNC);  
237 the growth of giant cloud condensation nuclei (CCN) (Barahona et al., 2010) (BA10) by  
238 introducing an additional condensation rate term to account for condensation of giant CCN (which



239 will reduce CDNC); as well as the modification of the original population splitting concept in  
240 FN05 and BA10 by Morales Betancourt and Nenes (2014) (MN14) by better accounting for the  
241 size of inertially limited CCN, and removing a discontinuity in the calculation of the surface area  
242 of cloud droplets.

243 The parameterization of Abdul Razzak and Ghan (2000) (ARG00) is used as the default  
244 aerosol activation module in WRF/Chem. It is not linked to the microphysics module or cumulus  
245 parameterization in WRF or WRF/Chem. However, for WRF/Chem, the cloud droplet number  
246 concentration (CDNC) generated in ARG00 is passed to the microphysics scheme, i.e., the  
247 Morrison two-moment microphysics scheme selected in this work.

### 248 **1.3 Motivations and Objectives**

249 The online-coupled meteorology and chemistry model, WRF/Chem, has recently been  
250 applied for air quality and climate modeling on a decadal scale (Yahya et al., 2016a, b).  
251 WRF/Chem can also simulate aerosol direct and indirect feedbacks, which are important  
252 considerations for climate modeling. However, as mentioned previously, the representations of  
253 OA and aerosol-cloud interactions in current regional and global climate models are subject to  
254 large uncertainties. In particular, while the VBS framework in WRF/Chem significantly improves  
255 SOA performance (Wang et al., 2015), it lacks the semi-volatile POA treatment, as well as  
256 fragmentation processes (Shrivastava et al., 2013). The first objective of this study is to reduce  
257 uncertainties associated with OA predictions by improving the existing VBS module in  
258 WRF/Chem and identifying the best gas-phase chemical mechanism to drive the VBS module for  
259 the most accurate OA predictions. The impact of the improved OA predictions on CDNC in  
260 WRF/Chem will be quantified. The second objective is to incorporate an improved aerosol  
261



262 activation parameterization based on the FN05 series into WRF/Chem to study its impacts on  
263 CDNC predictions.

## 264 **2. Model Configuration, Evaluation Protocol, and Observational Datasets**

265

### 266 **2.1. Model Setup and Inputs**

267

268 The model used in this study is a modified version of WRF/Chem v3.7.1 as described by Wang  
269 et al. (2015). The 2005 Carbon Bond gas-phase mechanism (CB05) of Yarwood et al. (2005) with  
270 additional chlorine chemistry is coupled with the Modal for Aerosol Dynamics in Europe –  
271 Secondary Organic Aerosol Model (MADE/SORGAM) (Ackermann et al., 1998; Schell et al.,  
272 2001) and the Volatility Basis Set (MADE/VBS) (Ahmadov et al., 2012). The CB05-VBS option  
273 has also been coupled to existing model treatments including the aerosol direct effect, the aerosol  
274 semi-direct effect on photolysis rates of major gases, and the aerosol indirect effect on CDNC and  
275 resulting impacts on shortwave radiation. The physics options used in WRF/Chem include the  
276 rapid and accurate radiative transfer model for GCM (RRTMG) for both shortwave and longwave  
277 radiation, the Yonsei University (YSU) planetary boundary layer (PBL) scheme (Hong et al., 2006;  
278 Hong, 2010), the Morrison et al. (2009) double moment microphysics scheme, as well as the Multi-  
279 scale Kain-Fritsch (MSKF) cumulus parameterization scheme (Zheng et al., 2016). Aqueous-  
280 phase chemistry module (AQCHEM) for both resolved and convective clouds is based on a similar  
281 AQCHEM module in CMAQv4.7 of Sarwar et al. (2011). The anthropogenic emissions used are  
282 from the 2010 emissions based on the 2008 U.S. Environmental Protection Agency (U.S. EPA)  
283 National Emissions Inventory (NEI) from the Air Quality Model Evaluation International Initiative  
284 (AQMEII) project (Pouliot et al., 2015). Dust emissions are based on the Atmospheric and  
285 Environmental Research Inc. and Air Force Weather Agency (AER/AFWA) scheme (Jones and  
286 Creighton, 2011). Emissions from sea salt are generated based on the scheme of Gong et al. (1997).





287 Biogenic emissions are simulated online by the Model of Emissions of Gases and Aerosols from  
288 Nature v2.1 (MEGAN2.1) (Guenther et al., 2006).

289 The chemical initial and boundary conditions (ICONS/BCONS) come from the modified  
290 CESM/CAM version 5.3 with updates by Gantt et al. (2014), He and Zhang (2014), and Glotfelty  
291 et al. (2016). The meteorological ICONS/BCONS are from the National Center for Environmental  
292 Protection Final Reanalyses (NCEP FNL) dataset, which is available every 6 hours. The chemical  
293 fields are also allowed to run continuously while the meteorology is reinitialized every 5 days. The  
294 simulations are performed at a horizontal resolution of 36-km with  $148 \times 112$  horizontal grid cells  
295 over the CONUS domain and parts of Canada and Mexico, and a vertical resolution of 34 layers  
296 from the surface to 100-hPa.

297 A number of sensitivity simulations are designed to identify the model configuration with  
298 results that are in the closest agreement to observations as well as the realistic model treatments of  
299 OA that are the closest to atmospheric processes. The baseline and sensitivity simulations are  
300 conducted from May to June 2010, during which the Nexus of Air Quality and Climate Change  
301 (CalNex) campaign was held in Bakersfield and Pasadena, California. The first 10 days from May  
302 1<sup>st</sup> to May 10<sup>th</sup> are considered to be the spin-up period.

## 303 **2.2. Model Evaluation Protocol and Available Measurements**

304  
305 Statistical measures including the Mean Bias (MB), Correlation Coefficient (Corr),  
306 Normalized Mean Bias (NMB) and Normalized Mean Error (NME) (Yu et al., 2006) are used to  
307 evaluate the simulations against observational data. Observational data are available for organic  
308 carbon (OC) and total carbon (TC) from the Speciated Trends Network (STN) and the Interagency  
309 Monitoring for Protected Visual Environments (IMPROVE). While both OC and TC from  
310 IMPROVE are used for model evaluation, only TC data from STN are used as STN uses the



311 thermo-optical transmittance protocol for OC that is different from the one used by IMPROVE  
312 (Zhang et al., 2012). In addition, the measurements for STN OC are not blank corrected for carbon  
313 on the background filter (Wang et al., 2012). The ratios OA/OC ratios vary across locations in the  
314 continental U.S. (CONUS) depending on whether the OA is dominated by secondary formation  
315 (Aitken et al., 2008) or it contains more aliphatic hydrocarbons (Turpin and Lim, 2001). In this  
316 study, two ratios, 1.4 and 2.1, are used to convert simulated OA to OC based on a number of  
317 literature (Turpin and Lim, 2001; Aitken et al., 2008; Xu et al., 2015). As the simulations are based  
318 on CONUS with varying OA properties (less or more oxidized OA), the use of two OA/OC ratios  
319 can represent the different types of OA present for all locations in the U.S. Spatial plots, time series  
320 plots at specific sites, as well as overlay plots are used to evaluate model performance. The  
321 IMPROVE sites chosen for the time series plots include the visibility-protected areas in Brigantine  
322 National Wildlife Refuge (NWR), NJ, Death Valley National Park (NP), CA, Swanquarter  
323 National Wildlife Refuge (NWR), NC, and the Tallgrass Prairie National Preserve, KS. The  
324 Brigantine NWR is a tidal wetland and has a shallow bay, the Death Valley NP is a desert, and the  
325 Swanquarter NWR is a coastal brackish marsh. The time series plots are made at four STN sites  
326 including two urban sites: in Washington, DC and Boise, ID, one industrial site in Tampa, FL, and  
327 one rural/agricultural site in Liberty, KS. SOA, hydroxyl radical (OH) and hydroperoxy radical  
328 ( $\text{HO}_2$ ) data are also available for May to June 2010 as part of the California Research at the Nexus  
329 of Air Quality and Climate Change (CalNex) campaign (Kleindienst et al., 2012; Lewandowski et  
330 al., 2013) in Bakersfield, CA and Pasadena, CA, which are both urban locations. The Bakersfield  
331 sampling site is located between the city center and areas of agricultural activity, while the  
332 Pasadena site is located at the California Institute of Technology campus within the Los Angeles  
333 metropolitan area to the southwest and mountains in the north (Baker et al., 2015).



334 POA/OA ratios are also used to evaluate the performance of the model. A number of studies  
335 have reported observed POA/OA ratios which range from 15% to 40% over CONUS. For  
336 example, over southeastern U.S., hydrocarbon-like OA (HOA) and cooking OA are found to  
337 contribute to 21 – 38% of total OA in urban sites (Xu et al., 2015). HOA and oxygenated OA  
338 (OOA) are found to account for 34% and 66% of measured OA from Pittsburgh in September 2002  
339 (Zhang et al., 2005). HOA and cooking OA are assumed to be synonymous to POA, and OOA is  
340 assumed to be synonymous to SOA. Particulate matter sampled during August and September  
341 2006 in Houston as part of the Texas Air Quality Study II Radical and Aerosol Measurement  
342 Project showed that approximately 32% of OA comes from HOA (Cleveland et al., 2012). Results  
343 from positive matrix factorization analysis from the Pasadena ground site during May and June  
344 2010 showed that the primary components contribute 29% of the total OA mass (Hayes et al.,  
345 2013). Based on Zhang et al. (2007), the percentages of HOA mass at urban sites in Riverside,  
346 CA, from mid-July to mid-August 2005, in Houston, TX, from mid-August to mid-September  
347 2000, and in New York City in July 2001 are 15%, 38%, and 30%, respectively. In addition, Zhang  
348 et al. (2011) compiled a large number of field campaigns across the globe where the average  
349 POA/OA ratios for urban, downwind and rural/remote areas are found to be 0.42, 0.18 and 0.10  
350 respectively.

351 For the aerosol activation sensitivity and production simulations, additional variables that will  
352 be analyzed in this study include maximum 1-hour and 8-hour O<sub>3</sub> against the Clean Air Status and  
353 Trends Network (CASTNET) and Air Quality System (AQS), aerosol optical depth (AOD),  
354 CDNC and cloud condensation nuclei (CCN) against MODIS.

### 355 **3. Model Development and Improvement**

356



357 A number of modifications have been made to the standard version of WRF/Chem model  
358 v3.7.1. Those modifications and treatments are described below.

### 359 **3.1. OA Treatments**

360  
361 The CB05-VBS treatment in the default WRF/Chem v3.7.1 assumes that POA is nonreactive  
362 and nonvolatile. In this study, POA is assumed to be semivolatile, and can undergo gas-particle  
363 partitioning, similar to anthropogenic SOA (ASOA) and biogenic SOA (BSOA) in VBS. While  
364 the volatility of ASOA and BSOA is represented by 4 bins with  $C^*$  from  $10^0$  to  $10^3 \mu\text{g m}^{-3}$ . The  
365 POA is distributed into 9 bins, with  $C^*$  from  $10^{-2}$  to  $10^6 \mu\text{g m}^{-3}$ , following the set-up of Shrivastava  
366 et al. (2011). The POA is oxidized to form semi-volatile OA (SVOA), which can also undergo  
367 gas-particle partitioning. For the POA, bin-resolved enthalpies of vaporizations are used, ranging  
368 from  $64 \text{ kJ mol}^{-1}$  for the 9<sup>th</sup> bin to  $112 \text{ kJ mol}^{-1}$  for the 1<sup>st</sup> bin according to Shrivastava et al. (2011).  
369 The default enthalpy of vaporization ( $\Delta H_{\text{vap}}$ ) for SOA in WRF/Chem is  $30 \text{ kJ mol}^{-1}$  according to  
370 Lane et al. (2008). A more accurate alternative is to use the  $\Delta H_{\text{vap}}$  values calculated from the semi-  
371 empirical correlation from Epstein et al. (2010):

$$372 \quad \Delta H_{\text{vap}} = -11 \log_{10} C^*_{300} + 129 \quad (1)$$

373 The values of  $\Delta H_{\text{vap}}$  Epstein et al. (2010) are used in a number of sensitivity simulations and final  
374 production simulation.

375 Shrivastava et al. (2013, 2015) also implemented several cases of fragmentation and  
376 functionalization (FF) processes into VBS. For this study, the FF set-up is similar to the method  
377 employed by Shrivastava et al. (2013), with the exception that fragmentation percentages of 10%,  
378 25%, and 50% are used in sensitivity simulations. Shrivastava et al. (2013) used fragmentation  
379 percentages of 50% (intermediate fragmentation) and 85% (high fragmentation) in his simulations  
380 over Mexico City. For example, for the 10% FF case, 10% of the mass in the VBS species is



381 functionalized and moved to the next lower volatility bin, 80% is fragmented and moved to the  
382 highest volatility bin, and the remaining 10% is fragmented and becomes more volatile than the  
383 highest volatility bin (i.e., it is lost from the current volatility bins). For the 50% FF case, 50% is  
384 functionalized and moved to the next lower volatility bin, 40% is fragmented and moved to the  
385 highest volatility bin, and 10% is lost.

386 Zhao et al. (2014) measured IVOCs in Pasadena, CA during CalNex and found that the  
387 concentrations of primary IVOCs are similar to those of single-ring aromatics, and they produce  
388 about 30% of newly formed SOA in the afternoon. With the semivolatile POA and FF cases in this  
389 study, additional IVOC and SVOC emissions are added as three times of the traditional POA  
390 emissions from NEI, to account for missing IVOC and SVOC species in the traditional POA  
391 emission inventory. The fraction of IVOC/SVOC emissions assigned to each volatility bin is  
392 summarized in Table 3.

393 The mass fraction of organics in each volatility bin determined in laboratory studies also differs  
394 significantly according to the sources of organics. For example, May et al. (2013a, b, c) has  
395 different volatility distributions of mass fractions of organics for gasoline vehicle exhaust, diesel  
396 exhaust, and biomass burning. To take into account the different sources of organic compounds  
397 into a single volatility distribution for the purpose of this work, a new volatility distribution is  
398 calculated based on the mass fractions reported by Shrivastava et al. (2011), May et al. (2013a, c)  
399 and the percentages of VOC emissions from various sources from the 2008 NEI. According to the  
400 2008 NEI report (Rao et al., 2013), total VOC emissions from stationary, mobile and fire  
401 (prescribed and wildfire) sources are ~7.6, ~5.6, and ~49.6 million tons, respectively. The  
402 corresponding percentages for VOC emissions are ~12%, ~9%, and ~79% for stationary, mobile,  
403 and fire sources, respectively. Based on the U.S. EPA (2013), the percentages of diesel emissions



404 from mobile sources are low compared to gasoline sources (~7% of total diesel and gasoline  
405 sources); they are thus not included in this study.

406 An example calculation for the mass fraction of the lowest volatility bin for POA and  
407 IVOC/SVOC emissions are as follows:

$$408 \quad \text{Log } C_{-2}^* (\text{at } 298\text{K}) = 0.04 \times 12\% + 0.14 \times 9\% + 0.79 \times 79\% = 0.1754 \quad (2)$$

409 where  $C_{-2}^*$  refers to the lowest volatility bin with a value of  $10^{-2} \mu\text{g m}^{-3}$ , 12%, 9%, and 79% refer  
410 to the percentages for VOC emissions from stationary, mobile, and fire sources, respectively from  
411 NEI, 0.04 refers to the original mass fraction for stationary emissions based on anthropogenic  
412 emissions from Shrivastava et al. (2011) for the lowest volatility bin with a value of  $10^{-2} \mu\text{g m}^{-3}$ ,  
413 0.14 refers to the original mass fraction for gasoline emissions from May et al. (2013a) for the  
414 lowest volatility bin with a value of  $10^{-2} \mu\text{g m}^{-3}$ , 0.2 refers to the original mass fraction for biomass  
415 burning emissions from May et al. (2013c) for the lowest volatility bin with a value of  $10^{-2} \mu\text{g m}^{-3}$ ,  
416 and 0.1754 refers to the newly-calculated mass fraction of POA and IVOC/SVOC emissions for  
417 this study. The mass fractions used by Shrivastava et al. (2011), May et al. (2013a, c), and this  
418 work can be found in Table 3.

### 419 **3.2. Gas-Phase Chemical Mechanisms**

420  
421 Three gas-phase mechanisms are used: CB05, CB6, and SAPRC07. The gas-phase  
422 mechanisms for CB6 and SAPRC07 are coupled to the MADE/VBS in WRF/Chem v3.7.1 in this  
423 work following the coupling of CB05 with MADE/VBS by Wang et al. (2014). The emissions for  
424 all cases are based on the CB05 chemical species from the 2010 emissions based on the 2008 NEI.  
425 For SAPRC07, slight modifications had to be made to account for the different VOC species or  
426 groups. The mapping of emission species from CB05 to SAPRC07 is based on the grouping of



427 species from emitdb.xls from Henderson et al. (2014) as well as from  
428 <http://www.cert.ucr.edu/~carter/emitdb/old-emitdb.htm>. CB05 emissions are used for the CB6  
429 case, with the exception of the VOCs including propane, benzene, ethyne, acetone, and ketone that  
430 are mapped based on fractions of existing CB05 VOCs according to Yarwood et al. (2010).

431 In VBS, the SOA precursors for CB6 are similar to those for CB05. The SOA precursors for  
432 CB05 (and therefore CB6) are mapped from the default SAPRC99 precursors by Wang et al.  
433 (2015). The SAPRC07 SOA precursors follow the existing mapping of SAPRC99-MOSAIC/VBS  
434 in WRF/Chem. The chemical equations and rate parameters from ENVIRON (2013) and Carter  
435 (2010) for CB6 and SAPRC07 gas-phase mechanisms, respectively, were included in the  
436 chem/KPP/mechanisms directory in WRF/Chem. The SAPRC07 gas-phase mechanism  
437 implemented in WRF/Chem in this case is the uncondensed and expanded version C, which  
438 includes reactions for peroxy radical operators (Carter, 2010). Species in both CB6-MADE/VBS  
439 and SAPRC07-MADE/VBS undergo dry deposition, aqueous chemistry, photolysis, and wet  
440 scavenging that are similar to CB05-MADE/VBS.

### 441 **3.3. Aerosol Activation**

442  
443 The FN05 series aerosol activation parameterizations (with the exclusion of MN14) have been  
444 incorporated into 3-D regional air quality models and global climate and Earth system models such  
445 as the WRF-Community Atmosphere Model version 5 (WRF-CAM5) (Zhang et al., 2015), and in  
446 the global-through-urban WRF/Chem (GU-WRF/Chem) (Zhang et al., 2012) and CESM (Gantt et  
447 al., 2014). In this study, the FN series parameterizations are incorporated into WRF/Chem  
448 following the methods of Gantt et al. (2014) and Zhang et al. (2015) as described in detail in Zhang  
449 et al. (2015). However, in WRF/Chem, the aerosol activation module is only linked to the  
450 microphysics module through the variable CDNC, which is read by the microphysics module. It



451 is not coupled to the cumulus parameterization scheme unlike in WRF-CAM5 and CESM. The  
452 FN05 series has been incorporated into module\_mixactivate.F in the physics directory in  
453 WRF/Chem. As BN07 involves the entrainment effect for convective clouds and has very small  
454 impacts on non-convective CDNC (Zhang et al., 2015), it is not included in this study. In addition,  
455 unlike Gantt et al. (2014) and Zhang et al. (2015), the KU09 treatment is also not included in this  
456 study as the empirical constants  $A_{FHH}$  and  $B_{FHH}$  used in the formulation, which are compound-  
457 specific, have not been experimentally determined for black carbon, although those constants have  
458 been determined for dust and confirmed by Laaksonen et al. (2016). The additional MN14  
459 treatment incorporated in this study involves a small modification to the original FN05 series  
460 parameterizations (without KU09), and helps to better account for the size of inertially limited  
461 CCN, and to remove a discontinuity in the calculation of the surface area of cloud droplets  
462 (Morales Betancourt and Nenes, 2014). The updated treatments are about 20% more  
463 computationally expensive to run as compared to ARG00 (Zhang et al., 2016), but capture the  
464 sensitivity of CDNC to all aspects of the aerosol with comparable accuracy to numerical parcel  
465 models, which was shown to be an underlying reason for biases from ARG (Morales Betancourt  
466 et al., 2014).

## 467 **4. Results and Discussions**

468

### 469 **4.1. Sensitivity Simulations with VBS Treatments Coupled with CB05**

470

471 As listed in Table 4, a number of sensitivity simulations are designed to identify the best model  
472 configuration for OA treatments with the closest agreement to observations over CONUS. Those  
473 sensitivity simulations consider (i) two SOA modules (MADE/SORGAM vs MADE/VBS), (ii)  
474 two types of VBS treatment for POA (nonvolatile POA vs. semivolatile POA), (iii) two  $\Delta H_{vap}$   
475 treatments (default vs. the semi-empirical  $\Delta H_{vap}$  equation by Epstein et al. (2010)), (iv) three





476 different percentages of functionalization and fragmentation (FF) (10%, 25%, and 50%), (v) three  
477 sets of POA emissions (default vs. 1.5 or 3 times the original NEI POA emissions), (vi) three  
478 different gas-phase mechanisms (CB05, CB6, and SAPRC07), and (vii) two different aerosol  
479 activation schemes (ARG00 vs. combinations of different aerosol activation schemes of the FN05  
480 series: FN05, FN05/BA10, and MN14) All simulations except for CB05-SORG-DH contain the  
481 VBS treatments for OA. CB05-SORG-DH and CB05-VBS-DH treat POA emissions as  
482 nonvolatile. In addition, the impact of two different cumulus parameterization schemes: Grell –  
483 Freitas (Grell and Freitas, 2014) and the Multi-scale Kain Fritsch (MSKF) (Zheng et al., 2016)  
484 scheme were also tested.

485 Table 5 summarizes the main statistics for all sensitivity simulations in terms of mean obs,  
486 mean sim, Corr, NMB, and NME for hourly OC and TC concentrations against IMPROVE and  
487 hourly TC concentrations against STN, respectively, over the whole CONUS domain. Figure 1  
488 compares the domain mean hourly averaged observed OC or TC concentrations based on  
489 IMPROVE and STN with simulated concentrations calculated based on the ratios of OA/OC 1.4  
490 and 2.1 for each sensitivity simulation. The domain mean hourly averaged obs OC concentration  
491 is  $0.88 \mu\text{g m}^{-3}$  for IMPROVE, and the domain mean hourly averaged obs TC concentration is  $1.03$   
492  $\mu\text{g m}^{-3}$  for IMPROVE and  $2.71 \mu\text{g m}^{-3}$  for STN. As shown in Figure 1, the simulation  
493 CB05\_SORG\_DH with the default SOA module SORG largely underpredicts OC and TC with the  
494 largest NMBs and NMEs and the lowest Corr as compared to all other simulations with a SOA  
495 module based on the VBS method. The remaining VBS simulations significantly reduce the biases  
496 and errors in OC and TC from CB05\_SORG\_DH and also improve the correlation. Compared to  
497 CB05\_SORG\_DH, CB05\_VBS\_DH with nonvolatile POA seems to perform relatively well in  
498 terms of NMBs and Corr against IMPROVE OC, IMPROVE TC, and STN TC.



499 Adding the semivolatile POA treatment with 1.5 times the NEI POA emissions  
500 (CB05\_POA\_DH) reduces simulated OC and TC concentrations as compared to CB05\_VBS\_DH,  
501 due to the loss of mass from the semivolatile POA. As the POA mass is reduced, less surface area  
502 is available for SOA precursors to condense onto, resulting in decreased OA (thus decreased OC  
503 and TC) for CB05\_POA\_DH. Using the semi-empirical correlation of Epstein et al. (2010) for  
504  $\Delta H_{\text{vap}}$  increases the OC and TC concentrations (CB05\_POA vs. CB05\_POA\_DH). Compared to  
505 the default  $\Delta H_{\text{vap}}$  of  $30 \text{ kJ mol}^{-1}$  used in CB05\_POA\_DH, the semi-empirical correlation of Epstein  
506 et al. (2010) gives much higher  $\Delta H_{\text{vap}}$  values, resulting in more of the organic vapors in the  
507 particulate phase than in the gas phase. Compared to CB05-POA, the simulations with various FF  
508 treatments decrease the OA concentrations, as part of the OA mass is fragmented to higher  
509 volatility bins. The 10% FF case (CB05\_10%FF) does not differ significantly from the no FF case  
510 (CB05\_POA). However, increasing the percentage of FF (from 10% to 25%, then to 50%)  
511 decreases the OA concentrations. The FF treatments, however, even if they are more representative  
512 of actual SOA atmospheric formation processes, reduce the Corr slightly (compared to the cases  
513 CB05\_POA and CB05-10%FF). By doubling the POA emissions (from 1.5 to 3.0 times the  
514 original POA NEI emissions) for the 25% FF case (CB05\_FF25%\_EM3), the predicted OC and  
515 TC concentrations are closer to the observations. When evaluated against IMPROVE OC,  
516 IMPROVE TC, and STN TC, among for simulations using CB05, the simulations  
517 CB05\_VBS\_DH, CB05\_POA, CB05\_FF10%, and CB05\_FF25%\_EM3 perform better than other  
518 cases. The differences in the OC and TC predictions from the simulations with different gas-phase  
519 mechanisms will be discussed later in Section 2.

520 Figure 2 shows the spatial distributions of simulated OC and TC concentrations overlaid with  
521 observed OC from IMPROVE and TC from STN for the case CB05\_25%FF\_EM3 for the two



522 OA/OC ratios. The model performs much better for IMPROVE OC with an OA/OC ratio of 2.1  
523 as compared to 1.4, especially over eastern U.S. where the use of an OA/OC ratio of 1.4 results in  
524 large overpredictions. However over the central U.S. and parts of the western U.S., the use of an  
525 OA/OC ratio of 1.4 shows slightly better predictions of IMPROVE OC compared to the use of  
526 OA/OC ratio of 2.1 that gives underpredictions of OC. On the other hand, the model performs  
527 better for STN OC with an OA/OC ratio of 1.4 as compared to 2.1. The use of an OA/OC ratio of  
528 1.4 gives better agreement with STN TC over eastern U.S. where the use of an OA/OC ratio of 2.1  
529 results in large underpredictions of TC. Evaluation of OC and TC against IMPROVE and STN,  
530 respectively, therefore depends heavily on the OA/OC ratio, which is site-specific. Therefore in  
531 more rural sites (IMPROVE), the OA/OC ratio is more likely to be high (~2.1) with more  
532 oxygenated OA, while in more urban sites (STN), the OA/OC ratio is more likely to be lower  
533 (~1.4) due to fresher emissions and less oxidized species.

534 Figure 3 shows the POA/OA ratios for six sensitivity simulations. As mentioned earlier, the  
535 observed ratio of POA/total OA is approximately 15% to 40% during the summer period over  
536 various locations in the CONUS. As SOA concentrations from field campaigns are sparse at  
537 different locations and at different time periods, the POA/OA ratio is used to evaluate the model's  
538 capability to reproduce POA and SOA concentrations. The simulation CB05\_SORG\_DH with  
539 default SORGAM SOA module largely overpredicts the POA/OA ratio, due to significant  
540 underpredictions of SOA. The simulations CB05\_VBS\_DH, CB05\_50%FF, and  
541 CB05\_25%FF\_EM3 with various VBS treatments all have POA/OA ratios that fall within the  
542 range of 0.15 to 0.4, with lower POA/OA ratios over more rural areas and higher POA/OA ratios  
543 over urban areas. CB05\_VBS\_DH, however, might give too high POA concentrations over the  
544 western portion of the domain as it does not consider POA to be semivolatile. Considering



545 semivolatile POA, however, without considering the fragmentation and functionalization  
546 processes in the simulation CB05\_POA results in too low POA/OA ratio ( $< 0.1$  over most areas).  
547 Similarly, the CB05\_FF25% case also results in a large portion of CONUS with POA/OA ratios  
548 of  $< 0.1$ , due to the loss of POA mass. CB05\_FF50%, however, predicts reasonable POA/OA  
549 ratios, even with fragmentation/functionalization due to balanced loss of both POA and SOA mass  
550 through fragmentation to higher volatility bins. The simulation CB05\_FF25%\_EM3 also improves  
551 from CB05\_FF25% by increasing the POA mass contributing to higher POA/OA ratios.

552 Figure 4 shows the observed and simulated temporal variations of SOA concentrations at the  
553 two CalNex sites: Bakersfield and Pasadena in CA from May to June 2010 for the simulations  
554 CB05\_SORM\_DH, CB05\_VBS\_DH, CB05\_25%FF\_EM3, CB6\_25%FF\_EM3, and  
555 SAPRC07\_25%FF\_EM3. There are large underpredictions of SOA by all runs on some days (e.g.  
556 May 15 – 16, June 2 – 6, June 13 – 14) likely due to missing SOA precursor emissions. Table 6  
557 shows the statistics of the simulations presented in Figure 4. The results using CB6 and SAPRC07  
558 gas-phase mechanisms will be discussed in section 4.2. The observed SOA was derived based on  
559 the tracer method of Kleindienst et al. (2012) which contains some uncertainties. For example, it  
560 assumes mass fraction of the tracers in secondary organic carbon is the same in the field as that in  
561 the laboratory, and the tracers are assumed to be inert and are unlikely to undergo oxidation in the  
562 atmosphere, which might not be the case. In addition, the SOA data from the CalNex campaign  
563 only consider contributions from a small number of precursors including biogenic precursors (i.e.,  
564 isoprene,  $\alpha$ -pinene, and  $\beta$ -caryophyllene), and the anthropogenic precursors (i.e., toluene,  
565 polycyclic aromatic hydrocarbons (PAHs) and methyl butenol (MBO)).

566 As shown in Figure 4 and Table 6, the simulation CB05\_SORG\_DH with the default  
567 SORGAM SOA module significantly underpredicts observed SOA concentrations at both sites.



568 The model configuration of CB05\_VBS\_DH has been used in a number of WRF/Chem  
569 simulations published in literature (e.g., Yahya et al., 2015a; Campbell et al., 2015; Wang et al.,  
570 2015a, b). At Bakersfield, the simulation CB05\_VBS\_DH overpredicts the SOA concentrations  
571 for almost all the days. The simulation CB05\_25%FF\_EM3, however, underpredicts the SOA  
572 concentrations at Bakersfield, especially in June. The CB05\_25%FF\_EM3 case also shows low  
573 SOA concentrations throughout May and June, without much variability in SOA concentrations,  
574 likely due to underestimations of original POA emissions at Bakersfield. As the S/IVOC emissions  
575 for CB05\_25%FF\_EM3 are a factor of 3 of the original POA emissions from NEI, if the original  
576 POA emissions from NEI are underestimated, the S/IVOC emissions will be low, resulting in low  
577 SOA concentrations due to low concentrations of condensable material. At Pasadena, both  
578 CB05\_VBS\_DH and CB05\_25%FF\_EM3 overpredict the obs SOA from May 15<sup>th</sup> to May 30<sup>th</sup>,  
579 but are unable to capture the high SOA concentrations from 2<sup>nd</sup> to 6<sup>th</sup> June. The CB05\_VBS\_DH  
580 case seems to perform better than the CB05\_25%FF\_EM3 case when observed SOA  
581 concentrations are high. The results from this study are consistent with those from Baker et al.  
582 (2015), which showed that measured PM<sub>2.5</sub> OC at Bakersfield is largely underpredicted compared  
583 to Pasadena. Baker et al. (2015), however, attributed to the underpredictions of OC at Bakersfield  
584 and Pasadena mainly to primary OC predicted by the baseline model, as compared to the Aerosol  
585 Mass Spectrometer measurements, suggesting that OC is mostly secondary in nature in Pasadena.  
586 In addition, as mentioned earlier, the simulated SOA from WRF/Chem does not consider  
587 contributions from all the SOA precursors identified by their trace compounds (e.g., the biogenic  
588 precursor, b-caryophyllene, and the anthropogenic precursor MBO, are not included in  
589 WRF/Chem), which can help to account for the discrepancies between the simulated and observed  
590 SOA concentrations.



591 4.2. Sensitivity of OA predictions to different gas-phase mechanisms

592

593 Figure 1 shows that CB05\_FF25%\_EM3 produces the highest OC and TC concentrations at

594 the IMPROVE sites, followed by CB6\_FF25%\_EM3 and SAPRC07\_FF25%\_EM3, while

595 CB6\_FF25%\_EM3 produces the highest TC concentrations at the STN sites. However, the

596 differences in domain-mean simulated OC and TC between the simulations with the three different

597 gas-phase mechanisms are small, compared to the differences in simulated OC and TC due to

598 differences in VBS treatments (e.g., nonvolatile vs. semivolatile POA). Figure 4 also shows that

599 there are not much differences between simulated SOA concentrations with different gas-phase

600 mechanisms at Bakersfield, but larger differences are found at Pasadena. . For example,

601 SAPRC07\_25%FF\_EM3 produces much higher SOA concentrations compared to

602 CB05\_25%FF\_EM3 and CB6\_25%FF\_EM3 at Pasadena on several days (e.g., June 6-8). Figure

603 5 shows the time series of hydroxyl radical (OH) mixing ratios as well as diurnal plots of OH and

604 hydroperoxyl radical (HO<sub>2</sub>) at Pasadena from the CalNex field campaign. The time series of HO<sub>2</sub>

605 is not shown due to irregularity of the observational data. The model is able to reproduce the

606 diurnal variation of OH radicals but significantly overpredicts the daytime and peak OH mixing

607 ratios, especially for CB05 and CB6. All gas-phase mechanisms underpredict OH mixing ratios at

608 night. Among all simulations, SAPRC07 produces the closest simulated OH mixing ratios

609 compared to CB05 and CB6 gives the largest overpredictions. Similarly, the HO<sub>2</sub> mixing ratios

610 are generally overpredicted by all gas-phase mechanisms with SAPRC07 performing the best. The

611 overpredictions in OH and HO<sub>2</sub> mixing ratios do not help explain the underpredictions of SOA for

612 several days at Pasadena where underpredictions of VOCs may be the main cause, which is

613 consistent with the findings of Baker et al. (2015).



614 Figure 6 shows spatial distributions of average concentrations of oxidants including ozone  
615 ( $O_3$ ), OH,  $HO_2$ , as well as the OA species including anthropogenic SOA (ASOA), biogenic SOA  
616 (BSOA), TSOA, and POA. SAPRC07-25%FF-EM3 produces the highest domain average  $O_3$   
617 mixing ratios but the lowest domain average OH+ $HO_2$  mixing ratios while CB6-25%FF-EM3  
618 produces the highest domain average and maximum OH+ $HO_2$  mixing ratios but the lowest domain  
619 average  $O_3$  mixing ratios. These findings are mostly consistent from literature. For example,  
620 maximum  $O_3$  and OH mixing ratios over the Los Angeles area are higher for CB6 compared to  
621 CB05, which are consistent with the results from Yarwood et al. (2010). SAPRC07 also generally  
622 produces higher  $O_3$  mixing ratios compared to CB05. However, average  $O_3$  mixing ratios from  
623 CB6 are expected to be higher than CB05 (rather than lower as shown in Figure 6), according to  
624 the study from Nopmongkol et al. (2012) which showed higher  $O_3$  mixing ratios over Europe for  
625 January and July using the Comprehensive Air Quality Model with Extensions (CAMx). CB6 is a  
626 relatively new gas-phase mechanism, there are very few studies that evaluated its performance  
627 over a longer period of time, e.g., for the whole summer, and over CONUS. In addition, there are  
628 other uncertainties in this study. For example, the emissions for CB05 are used for CB6, the  
629 additional explicit VOC species in CB6 such as benzene and acetylene are not considered, which  
630 can also contribute to  $O_3$  formation. In addition, most locations in the U.S. in 2010 are considered  
631 to be  $NO_x$ -limited with localized VOC-limited regimes from May to September (Campbell et al.,  
632 2015), which means that  $O_3$  formation is more likely to depend on  $NO_x$  rather than VOC  
633 concentrations.

634 Table 7 shows the statistics for maximum 1-hr and 8-hr  $O_3$  mixing ratios evaluated against  
635 CASTNET and AQS. CASTNET sites are mainly rural sites, while AQS consists of urban,  
636 suburban, and rural sites. As expected, SAPRC07 consistently produces the highest maximum 1-



637 hr and maximum 8-hr O<sub>3</sub> mixing ratios and overpredicts at AQS sites with an NMB of ~16%.  
638 However, SAPRC07 performs the best at CASTNET sites, as both CB05 and CB6 significantly  
639 underpredict maximum 1-hr and maximum 8-hr O<sub>3</sub> mixing ratios. At CASTNET sites, CB6  
640 performs the poorest with the largest underpredictions for both maximum 1-hr and 8-hr O<sub>3</sub> mixing  
641 ratios. However, CB6 predicts higher maximum 1-hr and 8-hr O<sub>3</sub> mixing ratios at AQS sites, while  
642 CB05 predicts the lowest maximum 1-hr and 8-hr O<sub>3</sub> mixing ratios at AQS sites. It is likely that  
643 CB6 predicts higher O<sub>3</sub> mixing ratios at more VOC-limited sites in urban areas, while CB05  
644 predicts higher O<sub>3</sub> mixing ratios at more NO<sub>x</sub>-limited areas, due to the improvement in VOC  
645 speciation in CB6 compared to CB05. Overall, however, CB05 has the highest Corr and the lowest  
646 NMEs for CASTNET maximum 1-hr and AQS maximum 1-hr and 8-hr O<sub>3</sub> mixing ratios. For  
647 PM<sub>2.5</sub> concentrations, CB6 produces the best performance against IMPROVE (highest Corr,  
648 lowest NMB and NME) while CB05 produces the best performance against STN (highest Corr  
649 and lowest NME). All 3 cases perform poorly for PM<sub>10</sub> against AQS, with large underpredictions  
650 due to the non-consideration of the coarse mode inorganic species in MADE-VBS treatments.

651 Anthropogenic SOA (ASOA) concentrations are lower for CB6 and SAPRC07 compared to  
652 CB05. This is likely partially due to the emissions which are mapped from CB05 to CB6 and  
653 SAPRC07. The CB05 emissions are not likely to account for all anthropogenic VOC emissions in  
654 CB6 and SAPRC07, resulting in lower ASOA concentrations for CB6 and SAPRC07 compared  
655 to CB05. Biogenic SOA (BSOA) concentrations, however, are the largest for CB6, followed by  
656 SAPRC07 and CB05. BSOA concentrations are likely the highest for CB6 due to the highest  
657 OH+HO<sub>2</sub> mixing ratios for CB6. The more extensive VOC representation and high O<sub>3</sub> mixing  
658 ratios for SAPRC07 also likely contribute to the high BSOA concentrations for SAPRC07





659 compared to CB05. However, overall, the total SOA (TSOA) and POA concentrations for all three  
660 gas-phase mechanisms do not vary much, resulting in similar OA concentrations.

661 Figures 7 and 8 show the time series of simulated vs, observed OC from IMPROVE and  
662 simulated vs, observed TC from STN at several representative sites over CONUS for the different  
663 gas-phase mechanisms. In general, at IMPROVE sites, CB05 gives the highest OC concentrations  
664 compared to CB6 and SAPRC07 most of the time, resulting in overpredictions of OC  
665 concentrations, while CB6 and SAPRC07 perform better against IMPROVE OC. The  
666 overpredictions of CB05 are likely due to overpredictions in ASOA (as CB05 produces the highest  
667 ASOA concentrations compared to CB6 and SAPRC07 as shown in Figure 6). As these sites are  
668 located in rural locations, the dominant SOA is likely to be BSOA, or downwind ASOA from more  
669 urban areas. With the exception of Death Valley NP, CA, the model performs relatively well in  
670 predicting IMPROVE OC concentrations. Simulations with all three gas phase mechanisms  
671 overpredict OC concentrations over several days in May in Brigantine NWR, Death Valley and  
672 Swanquarter, but is able to predict several of the peaks in June. All three gas-phase mechanisms,  
673 however, largely underpredict OC concentrations over Death Valley from May 21<sup>st</sup> to June 30<sup>th</sup>.  
674 As the Death Valley NP is a desert, the OC at Death Valley NP is most likely due to downwind  
675 OC transported from upwind locations, for which the model is not able to capture due to  
676 meteorological biases such as biases in wind fields. The differences between simulation results  
677 from the gas-phase mechanisms are smaller for STN TC compared to IMPROVE OC, probably  
678 due to similar elemental carbon (EC) concentrations for all gas-phase mechanisms, which can form  
679 a significant percentage of TC. In general, all simulations with the three gas-phase mechanisms  
680 also show similar trends (peaks and troughs) for simulated TC, likely due to influences from  
681 meteorological parameters such as wind and precipitation. Overall, all three simulations are also



682 able to predict the magnitude and trends of STN TC concentrations relatively well. Similarly,  
683 CB05 tends to produce the highest TC concentrations, however, CB6 also does produce the highest  
684 TC concentrations for several days, for example, for some days in May in Washington, DC and  
685 Tampa, FL, as well as in June in Liberty, KS, likely due to influences of BSOA where CB6  
686 produces the highest concentrations as shown in Figure 6.

### 687 **4.3. Impact of Different VBS treatments on CDNC**

688  
689 Table 7 shows the statistics for model evaluation for simulated CDNC against MODIS-derived  
690 CDNC from Bennartz (2007) for May to June 2010. All simulations underpredict CDNC due likely  
691 to underpredictions in PM and CCN concentrations and uncertainties and/or assumptions in the  
692 derived CDNC based on MODIS retrievals of cloud properties by Bennartz (2007) (Zhang et al.,  
693 2015). For example, Bennartz (2007) derived the CDNC from cloud optical depths and cloud  
694 effective radius assuming adiabatically-stratified clouds. Among all simulations with CB05,  
695 CB05\_SORG\_DH produces the lowest CDNC due to underestimated OA concentrations.  
696 Increasing the OA concentrations helps to reduce the negative biases for CDNC. There are small  
697 differences, however, among simulated CDNC with different VBS treatments for CB05 in CDNC  
698 predictions, with similar Corr ~ 0.29, NMBs of ~-29% to -27% and NMEs of ~ 47%. Figure 9  
699 shows the spatial differences in predictions in warm clouds between the several simulations and  
700 the simulation CB05\_VBS\_DH. CB05\_SORGAM\_DH gives the lower CDNC than  
701 CB05\_VBS\_DH, indicating that the VBS treatment in CB05\_VBS\_DH helps to increase CDNC  
702 significantly. While other simulations with semivolatile POA treatments further increase domain  
703 average CDNC comparing to CB05\_VBS\_DH, the differences between CDNC predictions from  
704 those simulations and CB05\_VBS\_DH are quite similar. In general, CDNC with the semivolatile



705 POA cases are higher over western U.S. but lower over eastern U.S. due to decreases in column  
706 OA concentrations for the semivolatile POA cases compared to CB05\_VBS\_DH over eastern U.S.

707 The large differences in CDNC predictions, however, are found between simulations with the  
708 different gas-phase mechanisms. SAPRC07\_25%FF\_EM3 has the largest negative bias (NMB of  
709 -52%) compared to all other simulations with CB05 and the simulation with CB6. Figure 10  
710 compares the spatial plots for CDNC predictions for simulations with different gas-phase  
711 mechanisms, as well as the surface spatial plots for total OA and inorganic PM<sub>2.5</sub> concentrations.  
712 The simulation with SAPRC07 shows significantly lower CDNC over northeastern U.S.  
713 comparing to CDNC predictions from the other two simulations. While all three simulations show  
714 similar total OA concentrations, large differences are found for their total inorganic PM<sub>2.5</sub>  
715 concentrations, with SAPRC07 producing the lowest domain mean and maximum total inorganic  
716 PM<sub>2.5</sub> concentrations. Compared to CB05 and CB6, the lower inorganic PM<sub>2.5</sub> concentrations  
717 simulated with SAPRC07 are likely due to the low OH+HO<sub>2</sub> mixing ratios for SAPRC07 as shown  
718 in Figure 6, resulting in a lower PM number concentration and lower cloud condensation nuclei  
719 (CCN), thus lower CDNC.

#### 720 **4.4.Sensitivity Simulations for Aerosol Activation Parameterizations**

721

722 Among all OA sensitivity simulations, the simulation CB05-25%FF-EM3 gives an overall best  
723 performance in terms of OC, TC, O<sub>3</sub>, PM<sub>2.5</sub>, and CDNC evaluation, it is thus selected to test various  
724 aerosol activation parameterizations. As listed in Table 4, four sensitivity simulations are designed  
725 to test the FN05 series aerosol activation parameterizations with improved treatments comparing  
726 to the default ARG00 aerosol activation parameterization. These sensitivity simulations include  
727 the default ARG00, the FN05, the combination of FN05 and BA10, and the MN14. These  
728 simulations use the MSKF scheme instead of the Morrison microphysics schemes in the previous



729 SOA runs as the MSKF scheme has a better correlation with MODIS CDNC as compared to the  
730 Morrison microphysics scheme. Table 8 summarizes the model evaluation results against MODIS-  
731 derived CDNC from Bennartz (2007). The simulation ARG00 underpredicts CDNC with an NMB  
732 of -35%. The FN05 series helps to reduce the underpredictions of CDNC significantly, because  
733 they in general give higher activation fractions compared to the ARG00 parameterization under  
734 most atmospheric conditions (Ghan et al., 2011). The addition of BA10 to the FN05 takes into  
735 account the effects of condensation on giant CCN, which reduces the CDNC predictions and leads  
736 to a negligible underprediction of CDNC (with an NMB of -0.8%) compared to a slight  
737 overprediction by the FN05 with an NMB of 7.1%. MN14, which revises the original population  
738 splitting method in FN05 and BA10, slightly increases the CDNC to an NMB of 4.2% comparing  
739 to the FN05/BA10 simulation. The trends in the predictions of FN05, BA10, and MN14 are  
740 consistent with the reported bias of ~+8%, -10% and -3%, respectively, by Morales Betancourt  
741 and Nenes (2014) against the CDNC concentrations simulated from the cloud parcel model.  
742 However, the Corr and NME are worse with the FN05 series and MN14. The NMEs are almost  
743 doubled for the FN05 series and MN14, compared to that from the default ARG00. Figure 11  
744 compares the spatial distributions of the simulated CDNC in warm clouds from ARG00, FN05  
745 series, and MN14 and the MODIS-derived CDNC from Bennartz (2007). As shown in Figure 11,  
746 the lower Corr and higher NMEs for the FN05 series as compared to ARG00 shown in Table 9, as  
747 compared to ARG00, are due to the large overpredictions over northeastern U.S. but  
748 underpredictions over other parts of the domain. The simulated CDNC from the default ARG00  
749 case is similar to that from Bennartz (2007) over eastern U.S., the underpredictions are mainly  
750 over western U.S. and over the ocean because of the known bias when large CCN are not present  
751 (Morales Betancourt et al., 2014). The simulations with the FN05 series increase CDNC where



752 CCN is high, i.e., over the northeastern U.S., resulting in overpredictions in CDNC over  
753 northeastern U.S., and does not help to improve CDNC predictions over other parts of the U.S. as  
754 well as over the ocean.

755 Figure 12 compares the simulated CCN and AOD from the CB05\_25%FF\_EM3 + MN14 case  
756 with those derived from the MODIS. The model largely underpredicts CCN, especially over the  
757 western part of the domain, which explains the large underprediction of CDNC also over the  
758 western part of the domain. Condensation of the available water vapor occurs over CCN which are  
759 concentrated over northeastern U.S., resulting in overpredictions of CDNC over northeastern U.S.  
760 The lack of CCN over the ocean and the western part of the domain is related to the  
761 underpredictions of AOD over the same areas. This indicates biases in number (and probably mass)  
762 concentrations of column PM concentrations, especially over the ocean and western U.S. PM<sub>2.5</sub>  
763 and PM<sub>10</sub> observational data are available over the surface and are both underpredicted, however,  
764 there are no observational data for column concentrations of PM<sub>2.5</sub> and PM<sub>10</sub> for evaluation.  
765 Improving the spatial distribution and magnitude of emissions for PM species and precursors for  
766 the model layers at the surface and above the surface can help improve AOD and CCN predictions,  
767 therefore CDNC predictions.

## 768 5. Summary and Conclusions

769  
770 Current regional air quality models including WRF/Chem have large uncertainties in modeling  
771 OA and aerosol-cloud feedback mechanisms such as the aerosol activation process. Comparing to  
772 the traditional OA method, the VBS treatment helps to improve OA predictions by reducing the  
773 underpredictions of OA. By including a semivolatile POA treatment, using a semi-empirical  
774 formation of Epstein et al. (2010) for  $\Delta H_{\text{vap}}$ , including 25% fragmentation and functionalization  
775 as well as including additional S/IVOC emissions, the VBS treatment in WRF/Chem simulates the



776 atmospheric OA formation processes more realistically and can perform relatively well in  
777 predictions of OC and TC against IMPROVE and STN. POA/OA ratios for the  
778 CB05\_25%FF\_EM3 and CB05\_FF50% treatments are within the range of POA/OA ratios of  
779 ~0.15 to 0.40 from literature. Compared to the simulation with default SORGAM SOA module,  
780 the simulations with various new VBS treatments also give better agreement with observed SOA  
781 at Bakersfield and Pasadena during the CalNex field campaign from May to June 2010. However,  
782 biases exist in those simulations with the VBS treatments due to several possible reasons, including  
783 underestimated POA emissions, underpredicted VOC concentrations, as well as differences in the  
784 SOA precursors used in the model and those contributing to the observed SOA concentrations.  
785 The simulations with different gas-phase mechanisms (i.e., CB05, CB6, and SAPRC07) produce  
786 in general different ASOA and BSOA concentrations. SAPRC07 produces the highest O<sub>3</sub> mixing  
787 ratios, while CB6 produces the lowest OH + HO<sub>2</sub> mixing ratios. CB6 also performs the best when  
788 evaluated against IMPROVE PM<sub>2.5</sub> while CB05 performs the best when evaluated against STN  
789 PM<sub>2.5</sub> concentrations. All 3 cases perform poorly against AQS PM<sub>10</sub> evaluation. Due to the  
790 significant differences between O<sub>3</sub>, OH, and HO<sub>2</sub> mixing ratios for the three gas-phase  
791 mechanisms, inorganic PM concentrations vary widely, especially between the carbon bond  
792 mechanisms (CB05 and CB6) and SAPRC07, resulting in significantly different predictions of  
793 CDNC. The CDNC predictions do not vary much among simulations with CB05 and different  
794 VBS treatments, for example, for simulations with nonvolatile vs. semivolatile POA, and with and  
795 without fragmentation and functionalization treatments. The simulation with SAPRC07 produces  
796 the lowest CDNC compared to those with CB05 and CB6, due to the lowest inorganic PM number  
797 and mass concentrations resulted from the lowest OH and HO<sub>2</sub> mixing ratios among all



798 simulations. CB05 gives the best performances when evaluated against CASTNET and AQS ozone  
799 mixing ratios, STN PM<sub>2.5</sub> concentrations and against MODIS CDNC.

800 With the default ARG00 treatment in the model, in general, all simulations with VBS  
801 treatments underpredict the MODIS-derived CDNC by Bennartz (2007). By including the FN05  
802 series (i.e., FN05, FN05/BA10, and MN14), the underpredictions for CDNC are greatly reduced.  
803 However, the correlation coefficient and errors are worse with the FN05 series, with large  
804 overpredictions over the northeastern U.S., where CCN is high. The model performs poorly for  
805 AOD and CCN, likely due to inaccuracies in spatial distribution and magnitudes of PM and PM  
806 precursor emissions in the model layers at the surface and above the surface. The CDNC  
807 predictions can be improved by improving AOD and CCN underpredictions over western U.S. and  
808 over the ocean.

#### 809 **Code and Data Availability**

810 The WRF/Chem v3.7.1 code used in this paper will be available upon request. The inputs  
811 including the meteorological files, meteorological initial and boundary conditions, chemical initial  
812 and boundary conditions, model setup and configuration, and the namelist setup and instructions  
813 on how to run the simulations for a 1-day test case, as well as a sample output for a 1-day test, can  
814 be provided upon request.

#### 815 **Acknowledgments**

816  
817 This study is funded by the National Science Foundation EaSM program (AGS-1049200) at  
818 NCSU. The emissions are taken from the 2008 NEI-derived emissions for 2010 provided by the  
819 U.S. EPA, Environment Canada, and Mexican Secretariat of the Environment and Natural  
820 Resources (Secretaría de Medio Ambiente y Recursos Naturales-SEMARNAT) and National  
821 Institute of Ecology (Instituto Nacional de Ecología-INE) as part of the Air Quality Model



822 Evaluation International Initiative (AQMEII). The authors acknowledge use of the WRF-Chem  
 823 preprocessor tool mozbc provided by the Atmospheric Chemistry Observations and Modeling Lab  
 824 (ACOM) of NCAR and the script to generate initial and boundary conditions for WRF based on  
 825 CESM results provided by Ruby Leung, PNNL. This work also used the Stampede Extreme  
 826 Science and Engineering Discovery Environment (XSEDE) high-performance computing support  
 827 which is supported by the National Science Foundation grant number ACI-1053575. The authors  
 828 also acknowledge high-performance computing support from Yellowstone (ark:/85065/d7wd3xhc)  
 829 provided by NCAR's Computational and Information Systems Laboratory, sponsored by the  
 830 National Science Foundation and Information Systems Laboratory.

### 831 **References**

- 832 Abdul-Razzak, H., and Ghan, S.J.: A parameterization of aerosol activation 2. Multiple aerosol  
 833 types, *J. Geophys. Res.*, 105, D5, 6837 – 6844, 2000.
- 834 Ackermann, I.J., Hass, H., Memmesheimer, M., Ebel, A., Binkowski, F.S., and Shankar, U.: Modal  
 835 aerosol dynamics model for Europe: Development and first applications, *Atmospheric  
 836 environment*, 32, No.17, 2981-2999, 1998.
- 837 Ahmadov, R., McKeen, S.A., Robinson, A.L., Bareini, R., Middlebrook, A.M., De Gouw, J.A.,  
 838 Meagher, J., Hsie, E.-Y., Edgerton, E., Shaw, S., and Trainer, M.: A volatility basis set model  
 839 for summertime secondary organic aerosols over the eastern United States in 2006, *J. Geophys.  
 840 Res.*, 117, doi:10.1029/2011JD016831, 2012.
- 841 Aitken, A.C., DeCarlo, P.F., Kroll, Worsnop, D.R., Huffman, J.A., Docherty, K.S., Ulbrich, I.M.,  
 842 Mohr, C., Kimmel, J.R., Sueper, D., Sun, Y., Zhang, Q., Trimborn, A., Northway, M.,  
 843 Ziemann, P.J., Canagaratna, M.R., Onasch, T.B., Alfarra, M.R., Prevot, A.S.H., Dommen, J.,  
 844 Duplissy, J., Metzger, A., Baltensperger, U., and Jimenez, J.L.: O/C and OM/OC Ratios of  
 845 primary, secondary, and ambient organic aerosols with high-resolution time-of-flight aerosol  
 846 mass spectrometry, *Environ. Sci. Technol.*, 42(12), 4478 – 4485, doi:10.1021/es703009q,  
 847 2008.
- 848 Atkinson, R., Baulch, D.L., Cox, R.A., Crowley, J.N., Hampson, R.F., Hynes, R.G., Jenkin, M.E.,  
 849 Kerr, J.A., Rossi, M.J., and Troe, J.: “Evaluated kinetic and photochemical data for  
 850 atmospheric chemistry - IUPAC subcommittee on gas kinetic data evaluation for atmospheric  
 851 chemistry.” July 2005 web version available from  
 852 <http://www.iupackinetic.ch.cam.ac.uk/index.html>, 2005.





- 853 Atkinson, R.A., Baulch, D.L., Cox, R.A., Crowley, J.N., Hampson, R.F., Hynes, R.G., Jenkin,  
854 M.E., Kerr, J.A., Rossi, M.J., and Troe, J.: “Evaluated kinetic and photochemical data for  
855 atmospheric chemistry - IUPAC subcommittee on gas kinetic data evaluation for atmospheric  
856 chemistry.” January 3, 2010 web version available at <http://www.iupac-kinetic.ch.cam.ac.uk/index.html>, 2010.  
857
- 858 Baker, K.R., Carlton, A.G., Kleindienst, T.E., Offenberg, J.H., Beaver, M.R., Gentner, D.R.,  
859 Goldstein, A.H., Hayes, P.L., Jimenez, J.L., Gilman, J.B., de Gouw, J.A., Woody, M.C., Pye,  
860 H.O.T., Kelly, J.T., Lewandowski, M., Jaoui, M., Stevens, P.S., Brune, W.H., Lin, Y-H.,  
861 Rubitschun, C.L., and Surratt, J.D.: Gas and aerosol carbon in California: comparison of  
862 measurements and model predictions in Pasadena and Bakersfield, *Atmos. Chem. Phys.*, 15,  
863 5243 – 5258, doi:10.5194/acp-15-5243-2015, 2015.
- 864 Barahona, D., and Nenes, A.: Parameterization of cloud droplet formation in large-scale models:  
865 Including effects of entrainment, *J. Geophys. Res.*, 112, D16206, doi:10.1029/2007JF008473,  
866 2007.
- 867 Barahona, D., West, R.E.L., Stier, P., Romakkaniemi, S., Kokkola, H., and Nenes, A.:  
868 Comprehensively accounting for the effect of giant CCN in cloud activation parameterizations,  
869 *Atmos. Chem. Phys.*, 10, 2467 – 2473, 2010.
- 870 Bennartz, R.: Global assessment of marine boundary layer cloud droplet number concentration  
871 from satellite, *J. Geophys. Res. Atmos.*, 112, D02201, doi:10.1029/2006JD007547, 2007.
- 872 Bergstrom, R., Denier van der Gon, H.A.C., Prevot, A.S.H., Yttri, K.E., and Simpson, D.:  
873 Modelling of organic aerosols over Europe (2002 – 2007) using a volatility basis set (VBS)  
874 framework: application of different assumptions regarding the formation of secondary organic  
875 aerosol, *Atmos. Chem. Phys.*, 12, 8499 – 8527, doi:10.5194/acp-12-8499-2012, 2012.
- 876 Boucher, O., Randall, D., Artaxo, P., Bretherton, C., Feingold, G., Forster, P., Kerminen, V.-M.,  
877 Kondo, Y., Liao, H., Lohmann, U., Rasch, P., Satheesh, S.K., Sherwood, S., Stevens, B., and  
878 Zhang, X.Y.: Clouds and Aerosols. In: *Climate Change 2013: The Physical Science Basis. Contribution of Working Group I to the Fifth Assessment Report of the Intergovernmental Panel on Climate Change* [Stocker, T.F., D. Qin, G.-K. Plattner, M. Tignor, S.K. Allen, J. Boschung, A. Nauels, Y. Xia, V. Bex and P.M. Midgley (eds.)]. Cambridge University Press, Cambridge, United Kingdom and New York, NY, USA, 2013.
- 883 Campbell, P., Zhang, Y., Yahya, K., Wang, K., Hogrefe, C., Pouliot, G., Knote, C., Hodzic, A.,  
884 San Jose, R., Perez, J.L., Jimenez Guerrero, P., Baro, R., and Makar, P.: A multi-model  
885 assessment for the 2006 and 2010 simulations under the Air Quality Model Evaluation  
886 International Initiative (AQMEII) phase 2 over North America: Part I. Indicators of the  
887 sensitivity of O<sub>3</sub> and PM<sub>2.5</sub> formation regimes, *Atmos. Environ.*, 115, 569 – 586, 2015.
- 888 Carter, W.P.L.: Implementation of the SAPRC-99 chemical mechanism into the models-3  
889 framework, Report to the US EPA (<http://www.cert.ucr.edu/~carter/pubs/s99mod3.pdf>), 2000.  
890 Last accessed, February 19, 2016.



- 891 Carter, W.P.L.: Development of the SAPRC07 chemical mechanism, *Atmos. Environ.*, 44, 5324  
892 – 5335, doi:10.1016/j.atmosenv.2010.01.026, 2010.
- 893 Chan, A.W.H., Kautzman, K.E., Chhabra, P.S., Surratt, J.D., Chan, M.N., Crouse, J.D., Kurten,  
894 A., Wennberg, P.O., Flagan, R.C., and Seinfeld, J.H.: Secondary organic aerosol formation  
895 from photooxidation of naphthalene and alkylnaphthalenes: implications for oxidation of  
896 intermediate volatility organic compounds (IVOCs), *Atmos. Chem. Phys.*, 9, 3049-3060, 2009.
- 897 Cleveland, M.J., Ziemba, L.D., Griffin, R.J., Dibb, J.E., Anderson, C.H., Lefer, B., and  
898 Rappengluck, B.: Characterization of urban aerosol using aerosol mass spectrometry and  
899 proton nuclear magnetic resonance spectroscopy, *Atmos. Environ.*, 54, 511 – 518,  
900 doi:10.1016/j.atmosenv.2012.02.074, 2012.
- 901 Donahue, N.M., Robinson, A.L., Stanier, C.O., and Pandis, S.N.: Coupled partitioning, dilution  
902 and chemical aging of semivolatile organics, *Environ. Sci. Tech.*, 40, 2635 – 2643, 2006.
- 903 Donahue, M.N., Robinson, A.L., and Pandis, S.N.: Atmospheric organic particulate matter: From  
904 smoke to secondary organic aerosol, *Atmos. Environ.* 43, 94-106, 2009.
- 905 Emmons, L.K., Walters, S., Hess, P.G., Lamarque, J.-F., Pfister, G.G., Fillmore, D., Granier, C.,  
906 Guenter, A., Kinnison, D., Laepple, T., Orlando, J., Tie, X., Tyndall, G., Wiedinmyer, C.,  
907 Baughcum, S.L., and Kloster, S.: Description and evaluation of the Model for Ozone and  
908 Related chemical Tracers, version 4 (MOZART-4), *Geosci. Model Dev.*, 3, 43 – 67, 2010.
- 909 ENVIRON: User's guide to the comprehensive air quality model with extensions, version 6, 2013.  
910 Available at [www.camx.com/files/camxusersguide\\_v6-10.pdf](http://www.camx.com/files/camxusersguide_v6-10.pdf)
- 911 Epstein, S.A., Riipinen, I., and Donahue, N.M.: A semiempirical correlation between enthalpy of  
912 vaporization and saturation concentration for organic aerosol, *Environ. Sci. Technol.*, 44, 743  
913 – 748, 2010.
- 914 Farina, S.C., Adams, P.J., and Pandis, S.N.: Modeling global secondary organic aerosol formation  
915 and processing with the volatility basis set: Implications for anthropogenic secondary organic  
916 aerosol, *J. Geophys. Res.*, 115, D09202, doi:10.1029/2009JD013046, 2010.
- 917 Fountoukis, C., and Nenes, A.: Continued development of a cloud droplet formation  
918 parameterization for global climate models, *J. Geophys. Res.*, 110, D11212,  
919 doi:10.1029/2004JD00591, 2005.
- 920 Gantt, B., He, J., Zhang, X., Zhang, Y., and Nenes, A.: Incorporation of advanced aerosol  
921 activation treatments into CESM/CAM5: model evaluation and impacts on aerosol indirect  
922 effects, *Atmos. Chem. Phys.*, 14, 7485 – 7497, doi:10.5194/acp-14-7485-2014, 2014.
- 923 Ghan, S.J., Abdul-Razzak, H., Nenes, A., Ming, Y., Liu, X., Ovchinnikov, M., Shipway, B.,  
924 Meskhidze, N., Xu, J., and Shi, X.: Droplet nucleation: Physically-based parameterizations and  
925 comparative evaluation, *J. Adv. Model. Earth Syst.*, 3, M10001, doi:10.1029/2011ms000074,  
926 2011.



- 927 Glotfelty, T., He, J. and Zhang, Y.: Updated organic aerosol treatments in CESM/CAM5:  
 928 development and initial application, in preparation, 2016.
- 929 Gong, S., Barrie, L.A. and Blanchet, J.P.: Modeling sea salt aerosols in the atmosphere: 1. Model  
 930 development, *J. Geophys. Res.*, 102, 3805-3818, doi:10.1029/96JD02953, 1997.
- 931 Grell, G.A. and Freitas, S.R.: A scale and aerosol aware stochastic convective parameterization  
 932 for weather and air quality modeling, *Atmos. Chem. Phys.*, 14, 5233-5250, doi:10.5194/acp-  
 933 14-5233-2014, 2014.
- 934 Grieshop, A.P., Logue, P., Donahue, J.M., Robinson, A.L., Laboratory investigation of  
 935 photochemical oxidation of organic aerosol from wood fires 1: measurement and simulation  
 936 of organic aerosol evolution, *Atmos. Chem. Phys.*, 9, 1263-1277, 2009.
- 937 Guenther, A., Kart, T., Harley, P., Wiedinmyer, C., Palmer, P.I. and Geron, C.: Estimates of global  
 938 terrestrial isoprene emissions using MEGAN (Model of Emissions of Gases and Aerosols from  
 939 Nature), *Atmos. Chem. Phys.*, 6, 3181-3210, 2006.
- 940 Hallquist, M., Wenger, J.C., Baltensperger, U., Rudich, Y., Simpson, D., Claeys, M., Dommen, J.,  
 941 Donahue, N.M., George, C., Goldstein, A.H., Hamilton, J.F., Herrman, H., Hoffman, T.,  
 942 Iinuma, Y., Jang, M., Jenkin, M.E., Jimenez, J.L., Kiendler-Scharr, A., Maenhaut, W.,  
 943 McFiggans, G., Mentel, T.F., Monod, A., Prevot, A.S.H., Seinfeld, J.H., Surratt, J.D.,  
 944 Szmigielski, R., and Wildt, J.: The formation, properties and impact of secondary organic  
 945 aerosol: current and emerging issues, *Atmos. Chem. Phys.*, 9, 5155 – 5236, 2009.
- 946 Hayes, P.L., Ortega, A.M., Cubison, M.J., Froyd, K.D., Zhao, Y., Cliff, S.S., Hu, W.W., Toohey,  
 947 D.W., Flynn, J.H., Lefer, B.L., Grossberg, N., Alvarez, S., Rappengluck, B., Taylor, J.W.,  
 948 Allan, J.D., Holloway, J.S., Gilman, J.B., Kuster, W.C., de Gouw, J.A., Massoli, P., Zhang,  
 949 X., Liu, J., Weber, R.J., Corrigan, A.L., Russell, L.M., Isaacman, G., Worton, D.R., Kreisberg,  
 950 N.M., Goldstein, A.H., Thalman, R., Waxman, E.M., Volkamer, R., Lin, Y.H., Surratt, J.D.,  
 951 Kleindienst, T.E., Offenberg, J.H., Dusanter, S., Griffith, S., Stevens, P.S., Brioude, J.,  
 952 Angevine, W.M., and Jimenez, J.L.: Organic aerosol composition and sources in Pasadena,  
 953 California during the 2010 CalNex campaign, *J. Geophys. Res. Atmos.*, 118, 9233–9257,  
 954 doi:[10.1002/jgrd.50530](https://doi.org/10.1002/jgrd.50530), 2013.
- 955 He, J., and Zhang, Y.: Improvement and further development in CESM/CAM5: gas-phase  
 956 chemistry and inorganic aerosol treatments, *Atmos. Chem. Phys.*, 14, 9171 – 9200,  
 957 doi:10.5194/acp-14-9171-2014, 2014.
- 958 Henderson, B.H., Akhtar, F., Pye, H.O.T., Napelenok, S.L., and Hutzell, W.T.: A database and  
 959 tool for boundary conditions for regional air quality modeling: description and evaluation,  
 960 *Geosci. Model Dev.*, 7, 339 – 360, doi:10.5194/gmd-7-339-2014, 2014.
- 961 Hodzic, A., Jimenez, J.L., Madronich, S., Canagaratna, M.R., DeCarlo, P.F., Kleinman, L., and  
 962 Fast, J.: Modeling organic aerosols in a megacity: potential contribution of semi-volatile and



- 963 intermediate volatility primary organic compounds to secondary organic aerosol formation,  
 964 *Atmos. Chem. Phys.*, 10, 5491-5514, 2010.
- 965 Hong, S.-Y., Noh, Y. and Dudhia, J.: A new vertical diffusion package with an explicit treatment  
 966 of entrainment processes, *Mon. Wea. Rev.*, 134, 2318-2341, 2006.
- 967 Hong, S.-Y.: A new stable boundary-layer mixing scheme and its impact on the simulated East  
 968 Asian summer monsoon, *Q.J.R. Meteorol. Soc.*, 136, 1481 – 1496, doi:0.1002/qj.665, 2010.
- 969 IUPAC: "Evaluated Kinetic and Photochemical Data". IUPAC Subcommittee on Gas Kinetic Data  
 970 Evaluation for Atmospheric Chemistry. Web Version. Available at  
 971 <http://www.iupackinetic.ch.cam.ac.uk>. Latest data sheets dated June, 2006.
- 972 Jathar, S.H., Farina, S.C., Robinson, A.L., and Adams, P.J.: The influence of semi-volatile and  
 973 reactive primary emissions on the abundance and properties of global organic aerosol, *Atmos.*  
 974 *Chem. Phys.*, 11, 7727 – 7746, doi:10.5194/acp-11-7727-2011, 2011.
- 975 Jimenez, J.L., Canagaratna, M.R., Donahue, N.M., Prevot, A.S.H., Zhang, Q., Kroll, J.H.,  
 976 DeCarlo, P.F., Allan, J.D., Coe, H., Ng, N.L., Aiken, A.C., Docherty, K.S., Ulbrich, I.M.,  
 977 Grieshop, A.P., Robinson, A.L., Duplissy, J., Smith, J.D., Wilson, K.R., Lanz, V.A., Hueglin,  
 978 C., Sun, Y.L., Tian, J., Laaksonen, A., Raatikainen, T., Rautiainen, J., Vaattovaara, P., Ehn,  
 979 M., Kulmala, M., Tomlinson, J.M., Collins, D.R., Cubison, M.J., Dunlea, E.J., Huffman, J.A.,  
 980 Onasch, T.B., Alfarra, M.R., Williams, P.I., Bower, K., Kondo, Y., Schneider, J., Drewnick,  
 981 F., Borrmann, S., Weimer, S., Demerjian, K., Salcedo, D., Cottrell, L., Griffin, R., Takami, A.,  
 982 Miyoshi, T., Hatakeyama, S., Shimojo, A., Sun, J.Y., Zhang, Y.M., Dzepina, K., Kimmel,  
 983 J.R., Sueper, D., Jayne, J.T., Herndon, S.C., Trimborn, A.M., Williams, L.R., Wood, E.C.,  
 984 Middlebrook, A.M., Kolb, C.E., Baltensperger, U., and Worsnop, D.R.: Evolution of Organic  
 985 Aerosols in the Atmosphere, *Science*, 326 (5959), 1525 – 1529, doi:10.1126/science.1180353,  
 986 2009.
- 987 Jones, S. and Creighton, G.: AFWA dust emission scheme for WRF/Chem-GOCART, 2011 WRF  
 988 workshop, June 20-24, Boulder, CO, USA, 2011.
- 989 Kim, Y., Sartelet, K., and Seigneur, C.: Formation of secondary aerosols over Europe: comparison  
 990 of two gas-phase mechanisms, *Atmos. Chem. Phys.*, 11, 583 – 598, doi:10.5194/acp-11-583-  
 991 2011, 2011.
- 992 Kleindienst, T.E., Jaoui, M., Lewandowski, M., Offenberg, J.H., and Docherty, K.S.: The  
 993 formation of SOA and chemical tracer compounds from the photooxidation of naphthalene and  
 994 its methyl analogs in the presence and absence of nitrogen oxides, *Atmos. Chem. Phys.*, 8711  
 995 – 8726, doi:10.5194/acp-12-8711-2012, 2012.
- 996 Laaksonen, A., Malila, J., Nenes, A., Hung, H.Mop., Chen, J.P.: Surface fractal dimension, water  
 997 adsorption efficiency, and cloud nucleation activity of insoluble aerosol, *Nat.Sci.Rep.*, 6,  
 998 25504, doi:10.1038/srep25504, 2016.



- 999 Lane, T.E., Donahue, N.M., and Pandis, S.N.: Simulating secondary organic aerosol formation  
1000 using the volatility basis-set approach in a chemical transport model, 42, 7439 – 7451, 2008.
- 1001 Lewandowski, M., Piletic, I.R., Kleindienst, T.E., Offenberg, J.H., Beaver, M.R., Jaoui, M.,  
1002 Docherty, K.S., and Edney, E.O.: Secondary organic aerosol characterisation at field sites  
1003 across the United States during the spring-summer period, Intern. J. Environ. Anal. Chem.,  
1004 doi:10.1080/030674, 2013.
- 1005 Li, J., Zhang, H., and Ying, Q.: Comparison of the SAPRC07 and SAPRC99 photochemical  
1006 mechanisms during a high ozone episode in Texas: Differences in concentrations, OH budget  
1007 and relative response factors, Atmos. Environ., 25 – 35, doi:10.1016/j.atmosenv.2012.02.034,  
1008 2012.
- 1009 Luecken, D.J., Phillips, S., Sarwar, G., and Jang, C.: Effects of using the CB05 vs. SAPRC99 vs.  
1010 CB4 chemical mechanism on model predictions: Ozone and gas-phase photochemical  
1011 precursor concentrations, Atmos. Environ., 42, 5805 – 5820, 2008.
- 1012 May, A.A., Presto, A.A., Hennigan, C.J., Nguyen, N.T., Gordon, T.D., and Robinson, A.L.: Gas-  
1013 particle partitioning of primary organic aerosol emissions: (1) Gasoline vehicle exhaust,  
1014 Atmos. Environ., 77, 128 – 139, 2013a.
- 1015 May, A.A., Presto, A.A., Hennigan, C.J., Nguyen, N.T., Gordon, T.D., and Robinson, A.L.: Gas-  
1016 particle partitioning of primary organic aerosol emissions: (2) Diesel vehicles, Environ. Sci.  
1017 Tech., 47, 8288 – 8296, 2013b.
- 1018 May, A.A., Levin, E.J.T., Hennigan, C.J., Riipinen, I., Lee, T., Collett Jr., J.R., Jimenez, J.L.,  
1019 Kreidenweis, S.M., and Robinson, A.L.: Gas-particle partitioning of primary organic aerosol  
1020 emissions, 3. Biomass burning, J. Geophys. Res., 118, 11327 – 11338, doi:10.1002/jgrd.50828,  
1021 2013c.
- 1022 Morales Betancourt, R., and Nenes, A.: Droplet activation parameterization: the population-  
1023 splitting concept revisited, Geosci. Model Dev., 7, 2345 – 2357, doi:10.5194/gmd-7-2345-  
1024 2014, 2014.
- 1025 Morrison, H., Thompson, G. and Tatarskii, V.: Impact of cloud microphysics on the development  
1026 of trailing stratiform precipitation in a simulated squall line: Comparison of One- and Two-  
1027 Moment Schemes, Mon. Wea. Rev., 137, 991-1007, 2009.
- 1028 Murphy, B.N., and Pandis, S.N.: Simulating the formation of semivolatile primary and secondary  
1029 organic aerosol in a regional chemical transport model, Environ. Sci. Technol., 2009, 43, 4722  
1030 – 4728, 2009.
- 1031 Myhre, G., Shindell, D., Breon, F.-M., Collins, W., Fuglestvedt, F., Huang, J., Koch, D.,  
1032 Lamarque, J.-F., Lee, D., Mendoza, B., Nakajima, T., Robock, A., Stephens, G., Takemura,  
1033 T., and Zhan, H.: Anthropogenic and Natural Radiative Forcing in: Climate Change 2013: The  
1034 Physical Science Basis. Contribution of Working Group I to the Fifth Assessment Report of



- 1035 the Intergovernmental Panel on Climate Change [Stocker, T.F., D. Qin, G.-K. Plattner, M.  
 1036 Tignor, S.K. Allen, J. Boschung, A. Nauels, Y. Xia, V. Bex and P.M. Midgley (eds.)].  
 1037 Cambridge University Press, Cambridge, United Kingdom and New York, NY, USA, 2013.
- 1038 Nenes, A. Ghan, S., Abdul-Razzak, H., Chuang, P.Y., and Seinfeld, J.: Kinetic limitations on cloud  
 1039 droplet formation and impact on cloud albedo, *Tellus* (2001), 53B, 133 – 149, 2001.
- 1040 Nopmongcol, U., Koo, B., Tai, E., Jung, J., Piyachaturawat, P., Emery, C., Yarwood, G., Pirovano,  
 1041 G., Mitsakou, C., and Kallos, G.: Modeling Europe with CAMx for the Air Quality Model  
 1042 Evaluation International Initiative (AQMEII), *Atmos. Environ.*, 53, 177 – 185, 2001.
- 1043 Odum, J.R., Hoffman, T., Bowman, F., Collins, D., Flagan, R.C., and Seinfeld, J.H.: Gas/Particle  
 1044 Partitioning and Secondary Organic Aerosol Yields, *Environ. Sci. Tech.*, 30(8), 2580 – 2585,  
 1045 doi:10.1021/es950943+, 1996.
- 1046 Pouliot, G., van der Gon, H.D., Kuenen, J., Makar, P., Zhang, J., and Moran, M.: Analysis of the  
 1047 emission inventories and model-ready emission datasets for Europe and North America for  
 1048 phase 2 of the AQMEII project, *Atmos. Environ.*, 115, 345 – 360, 2015.
- 1049 Pye, H. and Seinfeld, J.H.: A global perspective on aerosol from low-volatility organic compounds,  
 1050 *Atmos. Chem. Phys.*, 10, 4377 – 4401, doi:10.5194/acp-10-4377-2010, 2010.
- 1051 Rao, V., Tooly, L., and Drukenbrod, J.: 2008 National Emissions Inventory: Review, Analysis and  
 1052 Highlights, EPA-454/R-13-005, accessed online at  
 1053 <http://www.epa.gov/ttn/chief/net/2008report.pdf>, 2013, last access October 9<sup>th</sup>, 2015.
- 1054 Sander, S.P., Friedl, R.R., Golden, D.M., Kurylo, M.J., Huie, R.E., Orkin, V.L., Moortgat, G.K.,  
 1055 Ravishankara, A.R., Kolb, C.E., Molina, M.J., and Finlayson-Pitts, B.J.: Chemical Kinetics  
 1056 and Photochemical Data for use in Atmospheric Studies, Evaluation Number 14. NASA Jet  
 1057 Propulsion Laboratory. February. Available from  
 1058 <http://jpldataeval.jpl.nasa.gov/download.html>, 2013.
- 1059 Sander, S.P., Friedl, R.R., Golden, D.M., Kurylo, M.J., Moortgat, G.K., Wine, P.H.,  
 1060 Ravishankara, A.R., Kolb, C.E., Molina, M.J., Finlayson-Pitts, B.J., Huie, R.E., and Orkin,  
 1061 V.L.: “Chemical Kinetics and Photochemical Data for use in Atmospheric Studies, Evaluation  
 1062 Number 15. NASA Jet Propulsion Laboratory.” July. Available from  
 1063 <http://jpldataeval.jpl.nasa.gov/download.html>, 2006.
- 1064 Sarwar, G., Fahey, K., Napelenok, S., Roselle, S. and Mathur, R.: Examining the impact of CMAQ  
 1065 model updates on aerosol sulfate predictions, the 10<sup>th</sup> Annual CMAS Models-3 User’s  
 1066 Conference, October, Chapel Hill, NC, 2011.
- 1067 Schell B., Ackermann, I.J., Hass, H., Binkowski, F.S., and Ebel, A.: Modeling the formation of  
 1068 secondary organic aerosol within a comprehensive air quality model system, *J. Geophys.*  
 1069 *Res.* 106, 28275-28293, 2001.





- 1070 Shearer, S.M., Harley, R.A., Jin, L., and Brown, N.J.: Comparison of SAPRC99 and SAPRC07  
1071 mechanisms in photochemical modeling for central California, *Atmos. Environ.*, 46, 205 –  
1072 216, doi:10.1016/j.atmosenv.2011.09.079, 2012.
- 1073 Shrivastava, M.K., Lane, T.E., Donahue, N.M., Pandis, S.N., and Robinson, A.L.: Effects of gas  
1074 particle partitioning and aging of primary emissions on urban and regional organic aerosol  
1075 concentrations, *J. Geophys. Res.*, 113, D18301, doi:10.1029/2007JD009735, 2008.
- 1076 Shrivastava, M., Fast, J., Easter, R., Gustafson Jr., W.I., Zaveri, R.A., Jimenez, J.L., Saide, P. and  
1077 Hodzic, A.: Modeling organic aerosols in a megacity: comparison of simple and complex  
1078 representations of the volatility basis set approach, *Atmos. Chem. Phys.*, 11, 6639 – 6662,  
1079 doi:10.5194/acp-11-6639-2011, 2011.
- 1080 Shrivastava, M., Zelenyuk, A., Imre, D., Easter, R., Beranek, J., Zaveri, R.A., and Fast, J.:  
1081 Implications of low volatility SOA and gas-phase fragmentation reactions on SOA loadings  
1082 and their spatial and temporal evolution in the atmosphere, *J. Geophys. Res. Atmos.*, 118, 3328  
1083 – 3342, doi:10.1002/jgrd.50160, 2013.
- 1084 Shrivastava, M., Easter, R.C., Liu, X., Zelenyuk, A., Singh, B., Zhang, K., Ma, P.-L., Chand, D.,  
1085 Ghan, S., Jimenez, J.I., Zhang, Q., Fast, J., Rasch, P.J., and Titta, P.: Global transformation  
1086 and fate of SOA: Implications of low-volatility SOA and gas-phase fragmentation reactions,  
1087 *J. Geophys. Res. Atmos.*, 120, 4169 – 4195, doi:10.1002/2014JD022563, 2015.
- 1088 Stockwell, W., Kirchner, F., Kuhn, M., and Seefeld, S.: A new mechanism for regional  
1089 atmospheric chemistry modeling, *J. Geophys. Res.*, 102, D22, 25847 – 25879, 1997.
- 1090 Tsimpidi, A.P., Karydis, V.A., Zavala, M., Lei, W., Molina, L., Ulbrich, I.M., Jimenez, J.L., and  
1091 Pandis, S.N.: Evaluation of the volatility basis-set approach for the simulation of organic  
1092 aerosol formation in the Mexico City metropolitan area. *Atmospheric Chemistry and Physics*  
1093 10, 525-546, 2010.
- 1094 Turpin, B.J., and Lim, H.-J.: Species Contributions to PM<sub>2.5</sub> Mass concentrations: Revisiting  
1095 Common Assumptions for Estimating Organic Mass, *Aero. Sci. Technol.*, 35, 1, 602 – 610,  
1096 doi:10.1080/02786820119445, 2001.
- 1097 US EPA: 2008 National Emissions Inventory, version 3 Technical Support Document, September  
1098 2013, Draft, accessed online at  
1099 [http://www3.epa.gov/ttn/chief/net/2008neiv3/2008\\_neiv3\\_tsd\\_draft.pdf](http://www3.epa.gov/ttn/chief/net/2008neiv3/2008_neiv3_tsd_draft.pdf), 2013, last accessed  
1100 October 10<sup>th</sup>, 2015.
- 1101 Wang, K., and Zhang, Y.: Application, evaluation, and process analysis of the US EPA's 2002  
1102 Multiple-Pollutant Air Quality Modeling Platform, *Atmos. And Clim. Sci.*, 2, 254 – 289, 2012.
- 1103 Wang, K., Zhang, Y., Yahya, K., Wu, S.-Y., and Grell, G.: Implementation and initial application  
1104 of new chemistry-aerosol options in WRF/Chem for simulating secondary organic aerosols



- 1105 and aerosol indirect effects, *Atmos. Environ.*, 115, 716 – 723,  
1106 doi:10.1016/j.atmosenv.2015.12.007, 2015.
- 1107 Xu, L., Guo, H., Boyd, C.M., Klein, M., Bougiatioti, A., Cerully, K.M., Hite, J.R., Isaacman-  
1108 VanWertz, G., Kreisberg, N.M., Knote, C., Olson, K., Koss, A., Goldstein, A.H., Hering, S.V.,  
1109 de Gouw, J., Baumann, K., Lee, S.-H., Nenes, A., Weber, R.J., and Ng, N.L.: Effects of  
1110 anthropogenic emissions on aerosol formation from isoprene and monoterpenes in the  
1111 southeastern United States, *Proc. Natl. Acad. Sci.*, 112, 1, 37 – 42,  
1112 doi:10.1073/pnas.1417609112, 2015.
- 1113 Yahya, K., Wang, K., Campbell, P., Glotfelty, T., He, J., and Zhang, Y.: Decadal evaluation of  
1114 regional climate, air quality and their interactions over the continental US using WRF/Chem  
1115 version 3.6.1, *Geosci. Model Dev.*, 9, 671 – 695, doi:10.5194/gmd-9-671-2016, 2016a.
- 1116 Yahya, K., Campbell, P., Chen, Y., Glotfelty, T., Pirhalla, M., and Zhang, Y.: Downscaling CESM  
1117 using WRF/Chem: Decadal Application for Regional Air Quality and Climate Modeling over  
1118 the U.S. under the Representative Concentration Pathways Scenarios, in preparation, 2016b.
- 1119 Yarwood, G., Rao, S., Yocke, M., and Whitten, G.Z.: Final Report – Updates to the Carbon Bond  
1120 Chemical Mechanism: CB05, Rep. RT-04-00675, 246 pp., Yocke and Co., Novato, CA, 2005.
- 1121 Yarwood, G., Whitten, G.Z., Jung, J., Heo, G., and Allen, D.T.: Final Report – Development,  
1122 Evaluation and Testing of Version 6 of the Carbon Bond Chemical Mechanism (CB6): Work  
1123 Order No. 582-7-84005-FY10-26, ENVIRON, Novato, CA, 2010.
- 1124 Yu, S., Eder, B., Dennis, R., Chu, S.-H., and Schwartz, S.: New unbiased symmetric metrics for  
1125 evaluation of air quality models, *Atmos. Sci. Lett.*, 7, 26 – 34, 2006.
- 1126 Zhang, Q., Worsnop, D.R., Canagaratna, M.R., and Jimenez, J.L.: Hydrocarbon-like and  
1127 oxygenated organic aerosols in Pittsburgh: insight into sources and processes of organic  
1128 aerosols, *Atmos. Chem. Phys.*, 5, 3289 – 3311, doi:10.5194/acp-5-3289-2005, 2005.
- 1129 Zhang, Q., Jimenez, J.L., Canagaratna, M.R., Allan, J.D., Coe, H., Ulbrich, I., Alfarra, M.R.,  
1130 Takami, A., Middlebrook, A.M., Sun, Y.L., Dzepina, K., Dunlea, E., Docherty, K., DeCarlo,  
1131 P.F., Salcedo, D., Onasch, T., Jayne, J.T., Miyoshi, T., Shimojo, A., Hatakeyama, S.,  
1132 Takegawa, N., Kondo, Y., Schneider, J., Drewnick, F., Borrmann, S., Weimer, S., Demerjian,  
1133 K., Williams, P., Bower, K., Bahreini, R., Cottrell, L., Griffin, R.J., Rautiainen, J., Sun, J.Y.,  
1134 Zhang, Y.M., and Worsnop, D.R.: Ubiquity and dominance of oxygenated species in organic  
1135 aerosols in anthropogenically-influenced Northern Hemisphere midlatitudes, *Geophys. Res.  
1136 Lett.*, 34, L13801, doi:10.1029/2007GL029979, 2007.
- 1137 Zhang, Q., Jimenez, J.L., Canagaratna, M.R., Ulbrich, I.M., Ng, N.L., Worsnop, D.R., and Sun,  
1138 Y.: Understanding atmospheric organic aerosols via factor analysis of aerosol mass  
1139 spectrometry: a review, *Anal. Bioanal. Chem.*, 401(10), 3045 – 3067, doi:10.1007/s00216-  
1140 011-5355-y, 2011.





- 1141 Zhang, Y., Chen, Y.-C., Sarwar, G., and Schere, K.: Impact of gas-phase mechanisms on  
1142 WRF/Chem predictions: Mechanism implementation and comparative evaluation, *J. Geophys.*  
1143 *Res.*, 117, D01301, doi:10.1029/2011JD015775, 2012.
- 1144 Zhang, Y., Zhang, X., Wang, K., He, J., Leung, L.R., Fan, J., and Nenes, A.: Incorporating an  
1145 advanced aerosol activation parameterization into WRF-CAM5: Model evaluation and  
1146 parameterization intercomparison, *J. Geophys. Res. Atmos.*, 120, doi:10.1002/2014JD023051,  
1147 2015.
- 1148 Zhao, Y., Hennigan, C.J., May, A.A., Tkacik, D.S., de Gouw, J.A., Gilman, J.B., Kuster, W.C.,  
1149 Borbon, A., and Robinson, A.L.: Intermediate-volatility organic compounds: A large source  
1150 of secondary organic aerosol, *Environ. Sci. Technol.*, 48, 13743 – 13750,  
1151 doi:10.1021/es5035188, 2014.
- 1152 Zheng, Y., Alapaty, K.A., Herwehe, J.A., Del Genio, A.D., and Niyogi, D.: Improving high-  
1153 resolution weather forecasts using the Weather Research and Forecasting (WRF) Model with  
1154 an updated Kain-Fritsch scheme, *Mon. Wea. Rev.*, 144, 833 – 860, doi:10.1175/mwr-d-15-  
1155 0005.1, 2016.
- 1156
- 1157



Tables

Table 1. Summary of several literature studies of VBS treatments in various regional and global models.

Source	Ahmadov et al., 2012	Shrivastava et al., 2011	Farina et al., 2010	Jathar et al., 2011	Hodzic et al., 2010
<b>Model</b>	WRF-Chem	WRF-Chem	GISS II' GCM	GISS II' GCM	CHIMERE
<b>Domain</b>	CONUS	Mexico City	Global	Global	Mexico City
<b>Spatial Resolution</b>	20 km and 60 km	Nested 3 km within 12 km	4° × 5°	4° × 5°	5 km × 5 km and 35 km × 35 km
<b>Emissions of SVOCs, IVOCs, and VOCs</b>	Only VOCs; no emissions of SVOCs and IVOCs	SVOC emissions 3 times POA emissions for both anthropogenic and biomass burning emissions. IVOC emissions 1.5 times POA emissions	POA is treated as nonvolatile and nonreactive, but acts as absorbing phase for SOA condensation, forming 1 OA phase	SVOC emissions are represented by the traditional emission inventory. IVOC emissions are 1.5 times traditional emissions	SVOC emissions 3 times POA emissions. IVOC emissions 1.5 times POA emissions
<b>No. of VBS bins</b>	4	2 and 9	4	9	9
<b>Aging</b>	Yes and No Simulations with aging: each oxidation step produces 7.5% additional mass	Yes and No Simulations with aging: each oxidation step produces 15% additional mass	Yes	Yes and No. Each oxidation step does not produce any additional mass	Yes. 2 cases below: (i)Each oxidation step produces 7.5% additional mass (ii)Each oxidation step reduces the volatility by 2 orders of magnitude and 40% of additional mass produced
<b>Observational data</b>	SEARCH, STN, IMPROVE	MILAGRO 2006 field campaign	IMPROVE, EMEP	IMPROVE, FAME, MILAGRO, SOAR	MILAGRO 2006 field campaign
<b>Variables evaluated</b>	OC and EC	OA, HOA, OOA O:C ratio	OM:OC of 1.8	OA (surface), HOA, OOA	HOA, OOA, BBOA, O:C ratio
<b>Summary of results with VBS framework with/without aging compared to the traditional SOA approach</b>	-Improved diurnal variability -Results without the aging process underestimate OC throughout the day	-HOA and OOA: Lower negative bias with addition of S/IVOC emissions -OOA: 2 bin VBS better results than 9 bin VBS -Underprediction of O:C ratio in both cases	-IMPROVE: improved with aging -EMEP: aging further biases already high OA predictions	-Adding IVOC emissions improves performance, however underprediction remains in winter months	-HOA overpredicted during nighttime -Case(i): Modeled O:C 3 times lower than observed -Case(ii): Better agreement for O:C but SOA generally overestimated

Note: HOA: Hydrocarbon-like OA – Reduced specie of OA, generally understood as a surrogate for urban combustion-related POA; OOA: Oxygenated OA – Characterized by its high oxygen content and generally understood as a surrogate for SOA; BBOA: Biomass burning OA



Table 1. (cont). Summary of several literature studies of VBS treatments in various regional and global models.

Source	Bergstrom et al., 2012	Lane et al., 2008	Donahue et al., 2009	Murphy et al., 2009	This work
<b>Model</b>	EMEP	PMCAMx	PMCAMx	PMCAMx	WRF/Chem
<b>Domain</b>	Europe, a large part of the North Atlantic and Arctic areas	Eastern U.S.	Eastern U.S.	Eastern U.S.	CONUS with parts of Canada and Mexico
<b>Spatial Resolution</b>	50 km × 50 km	36 km × 36 km	NA	36 km × 36 km	36 km × 36 km
<b>Emissions of SVOCs, IVOCs and VOCs</b>	VOCs are present. S/IVOCs are 2.5 times the POA emissions	Only VOCs; SVOCs and IVOCs not added	Additional IVOCs added but details are not given	IVOC emissions are 0.2 to 0.8 times the nonvolatile POA emission rates	S/IVOCs are 1.5 to 3 times the nonvolatile POA NEI emissions
<b>No. of VBS bins</b>	4 for SOA components and 9 for POA	4	9	10	4 for SOA components and 9 for POA
<b>Aging</b>	Yes and No. Each oxidation step produces 7.5% additional mass	Yes. No additional mass produced for each oxidation step.	Yes. No additional mass produced for each oxidation step.	Yes. No additional mass produced for each oxidation step.	Yes. Each oxidation step produces 7.5% additional mass
<b>Observational data</b>	CARBOSOL, SORGA, Gote-2005	STN, IMPROVE	NA	STN, IMPROVE	STN, IMPROVE, field data
<b>Variables evaluated</b>	TC, OC	OA	POA, OPOA, SOA	OA	TC, OC, POA/OA
<b>Summary of results with VBS framework with/without aging compared to the traditional SOA approach</b>	-Addition of aging reactions improve summertime results but has little or negative consequences in wintertime -Deteriorations of model results with increased aging at urban influenced sites in southern Europe	-Addition of aging reactions overpredicts the OA concentrations in rural IMPROVE stations but improves the model performance in urban areas	-Aging results in better model predictions	-Slight overprediction with IMPROVE -Underprediction with STN	-Large improvements in predictions

Note: TC: total carbon; OC: Organic carbon; OPOA: oxidized POA



Table 2. Summary of main characteristics of CB05, CB6, and SAPRC07 gas-phase mechanisms.

	<b>CB05-Cl<sup>1</sup></b>	<b>CB6</b>	<b>SAPRC07<sup>2</sup></b>
<b>No. of species</b>	70	114	118
<b>No. of reactions</b>	156	218	599
<b>Lumping method</b>	Lumped structure based on carbon bonds	Lumped structure based on carbon bonds	Lumped species based on their reactivity towards hydroxyl (OH)
<b>Kinetic Data for rate constants</b>	Mostly from IUPAC (Atkinson et al., 2005). NASA/JPL (Sander et al., 2003) values were used in some cases where IUPAC data was not available.	New information from IUPAC (Atkinson et al., 2010) and NASA (Sander et al., 2006)	Mainly from IUPAC (2006) and NASA (Sander et al., 2006).
<b>Photolysis data</b>	Mainly from SAPRC99 chemical mechanism. IUPAC (Atkinson et al., 2005) was used if it differs significantly from SAPRC99.	New information from IUPAC (Atkinson et al., 2010) and NASA (Sander et al., 2006)	Mainly from IUPAC (2006) and NASA (Sander et al., 2006).
<b>Ozone chemistry</b>	Slightly underpredict O <sub>3</sub> mixing ratios with isoprene and in synthetic urban mixtures in chamber experiments.	Reduced underprediction in O <sub>3</sub> mixing ratios from benzene, toluene, and xylene, but forms O <sub>3</sub> from isoprene too slowly compared to CB05.	Slightly underpredict O <sub>3</sub> mixing ratios at low NO <sub>x</sub> levels in chamber experiments.
<b>Organic nitrate</b>	2 reactions involving organic nitrate (NTR).	Additional NO <sub>x</sub> recycling from organic nitrate to represent fate of NO <sub>x</sub> over multiple days.	Added peroxy+NO reactions to form organic nitrate.
<b>Chlorine chemistry</b>	20 additional reactions for Cl chemistry involving species Cl <sub>2</sub> , HOCl, Cl, ClO, and FMCl.	CB05 chlorine chemistry included in this work.	22 base chlorine reactions involving CL <sub>2</sub> , CLNO, CLONO, CLNO <sub>2</sub> , CLONO <sub>2</sub> , HOCl, and 26 additional reactions involving organic products
<b>Organic chemistry</b>	- Explicit organic aerosol precursors, e.g., isoprene, toluene, xylene, $\alpha$ -pinene, $\beta$ -pinene.	- Explicit long-lived and abundant organic compounds including propane, acetone, benzene and acetylene added - Extensive revision of isoprene and aromatics chemistry - Formation of alpha-dicarbonyl compounds (glyoxal, glycoaldehyde, methylglyoxal) - Updates to peroxy radical chemistry that will improve formation of H <sub>2</sub> O <sub>2</sub>	- Reformulated reactions of peroxy radicals so that effects of changes in NO <sub>x</sub> conditions on organic product formation is more accurately represented - Most comprehensive representation of VOCs compared to other gas-phase mechanisms
<b>3-D host models</b>	Implemented into WRF/Chem v3.6.1 by Wang et al. (2014). Also available in WRF/Chem v3.7.1	Implemented in CAMx by ENVIRON (2013)	Implemented in CMAQ (Carter, 2010)
<b>Reference</b>	Yarwood et al. (2005)	Yarwood et al. (2010) ENVIRON (2013)	Carter (2010)

<sup>1</sup> CB05 gas-phase mechanism with reactive chlorine chemistry (Yarwood et al., 2005)<sup>2</sup> SAPRC07 uncondensed and expanded version C, which includes reactions for peroxy radical operators (Carter, 2010).



Table 3. Factors to calculate S/IVOC emissions from POA emissions from Shrivastava et al. (2011), May et al. (2013a, c) and newly calculated factors for this study.

Log $C_i^*$ at 298K	Normalized fraction for stationary emissions based on anthropogenic emissions from Shrivastava et al. (2011)	Fraction for gasoline emissions from May et al. (2013a)	Fraction for biomass burning emissions from May et al. (2013c)	New calculated fraction for all sources based on Shrivastava et al. (2011), May et al. (2013a, c), and % distribution of NEI emissions
-2	0.04	0.14	0.2	0.1754
-1	0.02	0.13	0.0	0.0141
0	0.03	0.15	0.1	0.0961
1	0.05	0.26	0.1	0.1084
2	0.07	0.15	0.2	0.1799
3	0.11	0.03	0.1	0.0949
4	0.16	0.02	0.3	0.258
5	0.20	0.01	0.0	0.0249
6	0.32	0.11	0.0	0.0483



Table 4. Configurations for OA and aerosol activation sensitivity simulations. All simulations except for CB05-SORG-DH contain the VBS treatments for OA.

Name	Gas-Phase	$\Delta H_{\text{vap}}$	VBS	FF	POA emissions	Aerosol activation	Cumulus Scheme
CB05-SORG-DH	CB05	30 kJ mol <sup>-1</sup>	-	-	Original NEI	ARG00	Grell-Freitas
CB05-VBS-DH	CB05	30 kJ mol <sup>-1</sup>	SOA	-	Original NEI	ARG00	Grell-Freitas
CB05-POA-DH	CB05	30 kJ mol <sup>-1</sup>	SOA/POA	-	1.5×	ARG00	Grell-Freitas
CB05-POA	CB05	Epstein et al. (2010)	SOA/POA	-	1.5×	ARG00	Grell-Freitas
CB05-50%FF	CB05	Epstein et al. (2010)	SOA/POA	50%	1.5×	ARG00	Grell-Freitas
CB05-10%FF	CB05	Epstein et al. (2010)	SOA/POA	10%	1.5×	ARG00	Grell-Freitas
CB05-25%FF	CB05	Epstein et al. (2010)	SOA/POA	25%	1.5×	ARG00	Grell-Freitas
CB05-25%FF-EM3	CB05	Epstein et al. (2010)	SOA/POA	25%	3.0×	ARG00	Grell-Freitas
CB6-25%FF-EM3	CB6	Epstein et al. (2010)	SOA/POA	25%	3.0×	ARG00	Grell-Freitas
SAPRC07-25%FF-EM3	SAPRC07	Epstein et al. (2010)	SOA/POA	25%	3.0×	ARG00	Grell-Freitas
CB05-25%FF-EM3 (FN05)	CB05	Epstein et al. (2010)	SOA/POA	25%	3.0×	FN05	MSKF
CB05-25%FF-EM3 (FN05/BA10)	CB05	Epstein et al. (2010)	SOA/POA	25%	3.0×	FN05/BA10	MSKF
CB05-25%FF-EM3 (MN14)	CB05	Epstein et al. (2010)	SOA/POA	25%	3.0×	MN14	MSKF

The suffix “DH” in the case names refer to cases with the default  $\Delta H_{\text{vap}}$  of 30 kJ mol<sup>-1</sup>, otherwise with the semi-empirical correlation by Epstein et al. (2010). The simulations without the suffix “POA” indicate cases with nonvolatile default POA emissions. The suffix “POA” in the case names refer to cases with semivolatile POA. The suffix “FF” in the case names refer to cases with semivolatile POA and with fragmentation and functionalization treatments, and the suffix “EM3” in the case names refer to cases with 3 times the original NEI POA emissions to take into account for missing S/IVOC species. “-” indicates not applicable.



Table 5. Range of statistics for OA/OC ratios of 1.4 and 2.1 (1.4/ 2.1) for May to June 2010. All simulations use the ARG00 aerosol activation scheme and the Grell-Freitas cumulus parameterization.

Case	Mean Obs	Mean Sim	Corr	NMB (%)	NME (%)
<b>OC against IMPROVE</b>					
<b>CB05-SORG-DH</b>	0.88	0.28/ 0.19	0.26	-68.1/ -78.7	73.9/ 80.9
<b>CB05-VBS-DH</b>	0.88	1.19/ 0.79	0.51	34.9/ -10.1	75.5/ 52.3
<b>CB05-POA-DH</b>	0.88	0.89/ 0.59	0.51	1.1/ -32.6	52.4/ 59.0
<b>CB05-POA</b>	0.88	1.05/ 0.70	0.51	18.9/ -20.7	63.2/ 49.2
<b>CB05-10%FF</b>	0.88	1.05/ 0.70	0.51	19.4/ -20.4	63.0/ 49.1
<b>CB05-25%FF</b>	0.88	0.86/ 0.57	0.49	-2.9/ -35.2	54.6/ 51.4
<b>CB05-50%FF</b>	0.88	0.56/ 0.37	0.45	-36.4/ -57.6	54.4/ 62.6
<b>CB05-25%FF-EM3</b>	0.88	1.09/ 0.73	0.47	23.8/ -17.5	65.9/ 50.2
<b>CB6-25%FF-EM3</b>	0.88	1.06/ 0.71	0.48	20.5/ -19.6	49.4/ 63.7
<b>SAPRC07-25%FF-EM3</b>	0.88	1.00/ 0.67	0.46	13.3/ -24.4	60.1/ 50.4
<b>TC against IMPROVE</b>					
<b>CB05-SORG-DH</b>	1.03	0.44/ 0.34	0.30	-57.6/ -66.7	67.9/ 72.3
<b>CB05-VBS-DH</b>	1.03	1.34/ 0.94	0.52	30.6/ -8.0	70.3/ 51.1
<b>CB05-POA-DH</b>	1.03	1.13/ 0.83	0.52	10.2/ -18.7	58.5/ 48.7
<b>CB05-POA</b>	1.03	1.29/ 0.94	0.53	25.6/ -8.5	63.8/ 48.3
<b>CB05-10%FF</b>	1.03	1.29/ 0.94	0.53	25.9/ -8.2	63.8/ 48.2
<b>CB05-25%FF</b>	1.03	1.09/ 0.83	0.51	6.8/ -21.6	55.2/ 48.2
<b>CB05-50%FF</b>	1.03	0.80/ 0.61	0.47	-22.0/ -40.2	50.8/ 53.4
<b>CB05-25%FF-EM3</b>	1.03	1.32/ 0.97	0.49	29.7/ -5.7	50.7/ 66.9
<b>CB6-25%FF-EM3</b>	1.03	1.30/ 0.95	0.50	27.2/ -7.3	65.2/ 50.0
<b>SAPRC07-25%FF-EM3</b>	1.03	1.23/ 0.90	0.48	20.6/ -11.9	61.4/ 49.4
<b>TC against STN</b>					
<b>CB05-SORG-DH</b>	2.71	1.34/ 1.10	0.29	-50.6/ -59.4	60.1/ 64.9
<b>CB05-VBS-DH</b>	2.71	3.35/ 2.44	0.47	23.7/ -5.8	53.1/ 42.0
<b>CB05-POA-DH</b>	2.71	2.88/ 2.19	0.47	6.2/ -19.0	45.5/ 41.6
<b>CB05-POA</b>	2.71	3.03/ 2.30	0.46	11.7/ -15.3	44.6/ 39.9
<b>CB05-10%FF</b>	2.71	3.03/ 2.30	0.46	11.8/ -15.3	44.5/ 39.8
<b>CB05-25%-FF</b>	2.71	2.66/ 2.05	0.44	-1.8/ -24.3	41.5/ 42.0
<b>CB05-50%-FF</b>	2.71	2.07/ 1.65	0.39	-23.8/ -39.1	43.9/ 49.4
<b>CB05-25%FF-EM3</b>	2.71	3.27/ 2.45	0.41	20.5/ -9.5	49.7/ 41.7
<b>CB6-25%FF-EM3</b>	2.71	3.39/ 2.45	0.34	24.9/ -6.4	54.8/ 45.5
<b>SAPRC07-25%FF-EM3</b>	2.71	3.00/ 2.28	0.41	10.7/ -16.1	45.2/ 42.0



Table 6. Statistics for evaluation at Bakersfield and Pasadena sites. A bar chart of daily average obs vs. sim values can be found in Figure 4.

Case	Mean Obs	Mean Sim	Corr	NMB (%)	NME (%)
<b>Bakersfield</b>					
<b>CB05-SORG-DH</b>	0.51	5.9e-04	-0.15	-100	100%
<b>CB05-VBS-DH</b>	0.51	0.67	0.41	32.5	62.0
<b>CB05-25%FF-EM3</b>	0.51	0.24	-0.01	-52.0	61.0
<b>CB6-25%FF-EM3</b>	0.51	0.28	-0.04	-45.8	59.0
<b>SAPRC07-25%FF-EM3</b>	0.51	0.24	-0.16	-53.1	63.0
<b>Pasadena</b>					
<b>CB05-SORG-DH</b>	0.63	0.04	-0.07	-94.0	94.0
<b>CB05-VBS-DH</b>	0.63	0.54	0.09	-14.5	64.3
<b>CB05-25%FF-EM3</b>	0.63	0.54	-0.2	-14.4	66.2
<b>CB6-25%FF-EM3</b>	0.63	0.62	-0.2	-2.1	70.0
<b>SAPRC07-25%FF-EM3</b>	0.63	0.62	0.03	-1.4	70.5





Table 7. Statistics for max 1-h and max 8-h O<sub>3</sub> for simulations with different gas-phases against CASTNET and AQS for May to June 2010.

CASTNET Max 1-h O <sub>3</sub>					
Case	Mean Obs	Mean Sim	Corr	NMB (%)	NME (%)
CB05-25%FF-EM3	51.8	43.3	0.54	-16.3	21.9
CB6-25%FF-EM3	51.8	41.9	0.52	-19.1	24.1
SAPRC07-25%FF-EM3	51.8	48.3	0.51	-6.7	21.1
CASTNET Max 8-h O <sub>3</sub>					
Case	Mean Obs	Mean Sim	Corr	NMB (%)	NME (%)
CB05-25%FF-EM3	47.4	43.0	0.54	-9.3	18.9
CB6-25%FF-EM3	47.4	41.8	0.53	-11.8	20.6
SAPRC07-25%FF-EM3	47.4	47.9	0.50	1.0	19.8
AQS Max 1-h O <sub>3</sub>					
Case	Mean Obs	Mean Sim	Corr	NMB (%)	NME (%)
CB05-25%FF-EM3	51.0	49.9	0.55	-2.1	18.2
CB6-25%FF-EM3	51.0	51.5	0.43	1.0	20.8
SAPRC07-25%FF-EM3	51.0	59.3	0.44	16.4	26.1
AQS Max 8-h O <sub>3</sub>					
Case	Mean Obs	Mean Sim	Corr	NMB (%)	NME (%)
CB05-25%FF-EM3	46.2	46.0	0.54	-0.4	18.6
CB6-25%FF-EM3	46.2	47.4	0.47	2.6	20.3
SAPRC07-25%FF-EM3	46.2	53.7	0.46	16.3	25.4
IMPROVE PM <sub>2.5</sub>					
Case	Mean Obs	Mean Sim	Corr	NMB (%)	NME (%)
CB05-25%FF-EM3	4.9	3.8	0.64	-22.0	40.6
CB6-25%FF-EM3	4.9	4.1	0.65	-16.5	39.6
SAPRC07-25%FF-EM3	4.9	3.5	0.60	-28.5	42.9
STN PM <sub>2.5</sub>					
Case	Mean Obs	Mean Sim	Corr	NMB (%)	NME (%)
CB05-25%FF-EM3	11.1	8.8	0.48	-20.6	40.7
CB6-25%FF-EM3	11.1	10.0	0.37	-9.3	44.3
SAPRC07-25%FF-EM3	11.1	7.7	0.40	-30.5	45.2
AQS PM <sub>10</sub>					
Case	Mean Obs	Mean Sim	Corr	NMB (%)	NME (%)
CB05-25%FF-EM3	24.6	7.3	0.08	-70.2	73.5
CB6-25%FF-EM3	24.6	8.0	0.09	-67.7	71.8
SAPRC07-25%FF-EM3	24.6	6.9	0.09	-71.9	74.8



Table 8. Statistics for model evaluation for simulated CDNC against MODIS-derived CDNC from Bennartz (2007).

Case	Mean Obs	Mean Sim	Corr	NMB (%)	NME (%)
<b>CB05-SORG-DH</b>	162.1	96.0	0.28	-40.8	50.4
<b>CB05-VBS-DH</b>	162.1	106.0	0.28	-34.6	50.6
<b>CB05-POA-DH</b>	162.1	115.0	0.29	-29.1	47.4
<b>CB05-POA</b>	162.1	117.3	0.29	-27.7	47.3
<b>CB05-10%FF</b>	162.1	117.1	0.29	-27.8	47.2
<b>CB05-25%-FF</b>	162.1	116.4	0.29	-28.2	47.3
<b>CB05-50%-FF</b>	162.1	114.7	0.29	-29.2	47.4
<b>CB05-25%FF-EM3</b>	162.1	116.2	0.29	-28.3	47.3
<b>CB6-25%FF-EM3</b>	162.1	110.4	0.30	-31.9	47.3
<b>SAPRC07-25%FF-EM3</b>	162.1	77.3	0.26	-52.3	55.8

Table 9. Statistics for simulated CDNC for CB05-25%FF-EM3 against MODIS-derived CDNC from Bennartz (2007) for May to June 2010.

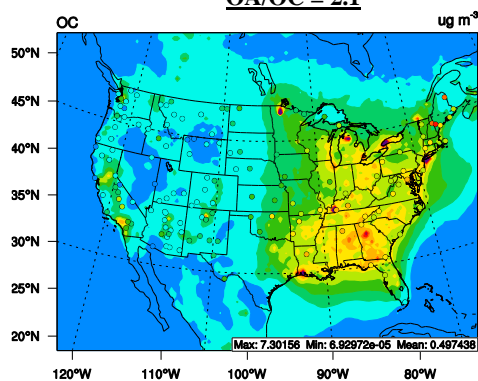
Case	Mean Obs	Mean Sim	Corr	NMB (%)	NME (%)
<b>ARG00</b>	162.1	104.8	0.31	-35.4	49.9
<b>FN05</b>	162.1	173.8	0.26	7.1	93.0
<b>FN05/BA10</b>	162.1	160.8	0.27	-0.8	87.9
<b>MN14</b>	162.1	168.9	0.27	4.2	89.6



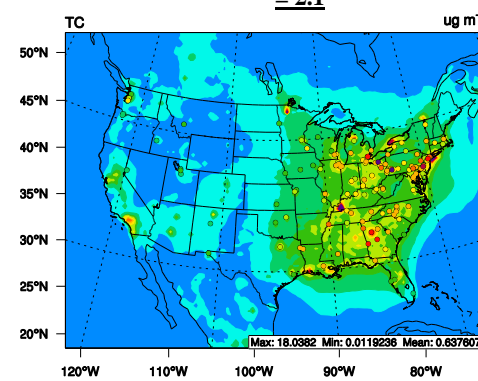
Figure 1. Sim OC and TC concentrations against observations from IMPROVE and STN under two A/O ratios: 1.4 and 2.1, , resulting in a range of possible OC or TC values denoted by the gray bars. The obs OC or TC is denoted by the horizontal dotted line.



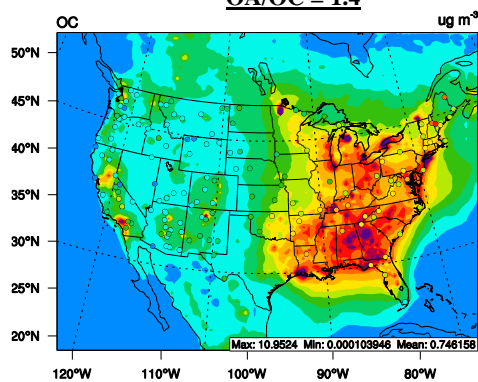
**IMPROVE OC (markers) with Sim OC (background) with  
 OA/OC = 2.1**



**STN TC (markers) with Sim TC (background) with OA/OC  
 = 2.1**



**IMPROVE OC (markers) with Sim OC (background) with  
 OA/OC = 1.4**



**STN TC (markers) with Sim TC (background) with OA/OC  
 = 1.4**

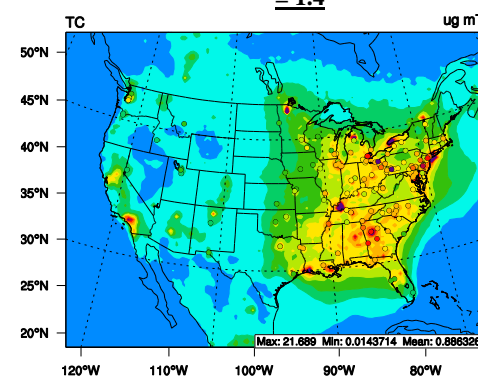


Figure 2. Overlay of obs data (markers) vs. sim data (background) for IMPROVE OC and STN TC and for OA/OC ratios of 1.4 and 2.1 for the case CB05\_25%FF\_EM3.

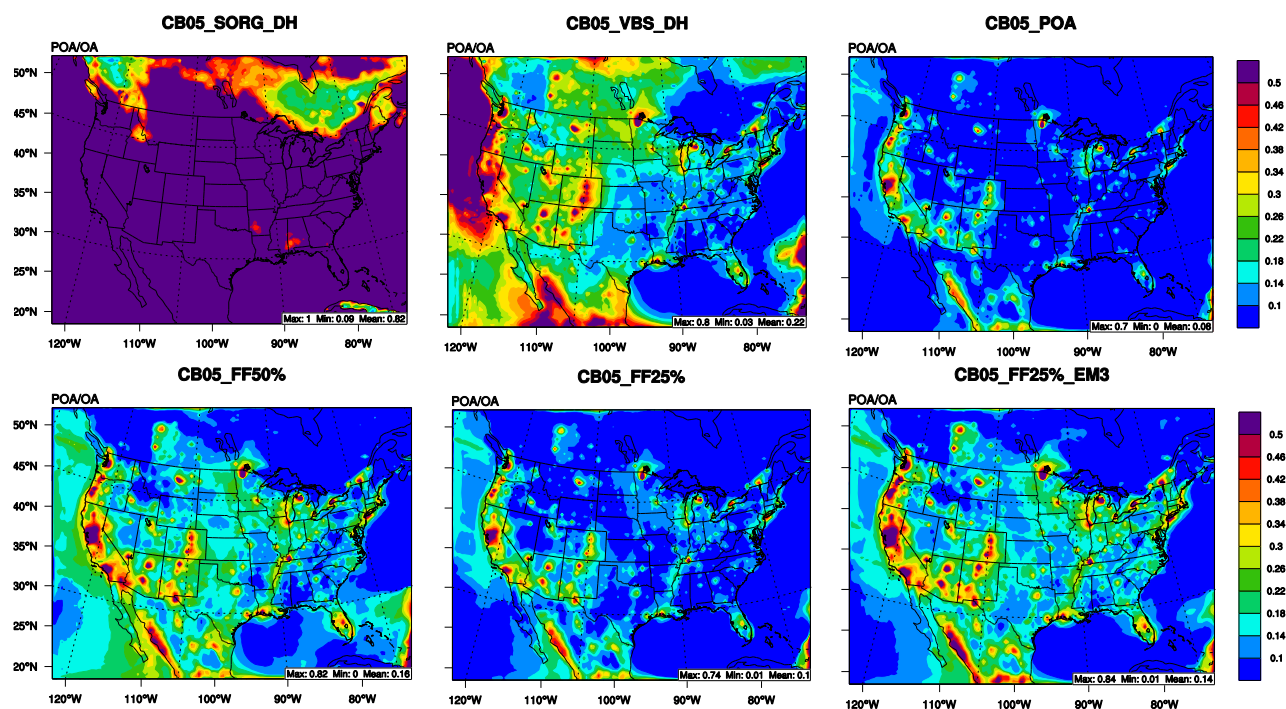


Figure 3. POA/OA ratios of sim data from various sensitivity simulation cases.

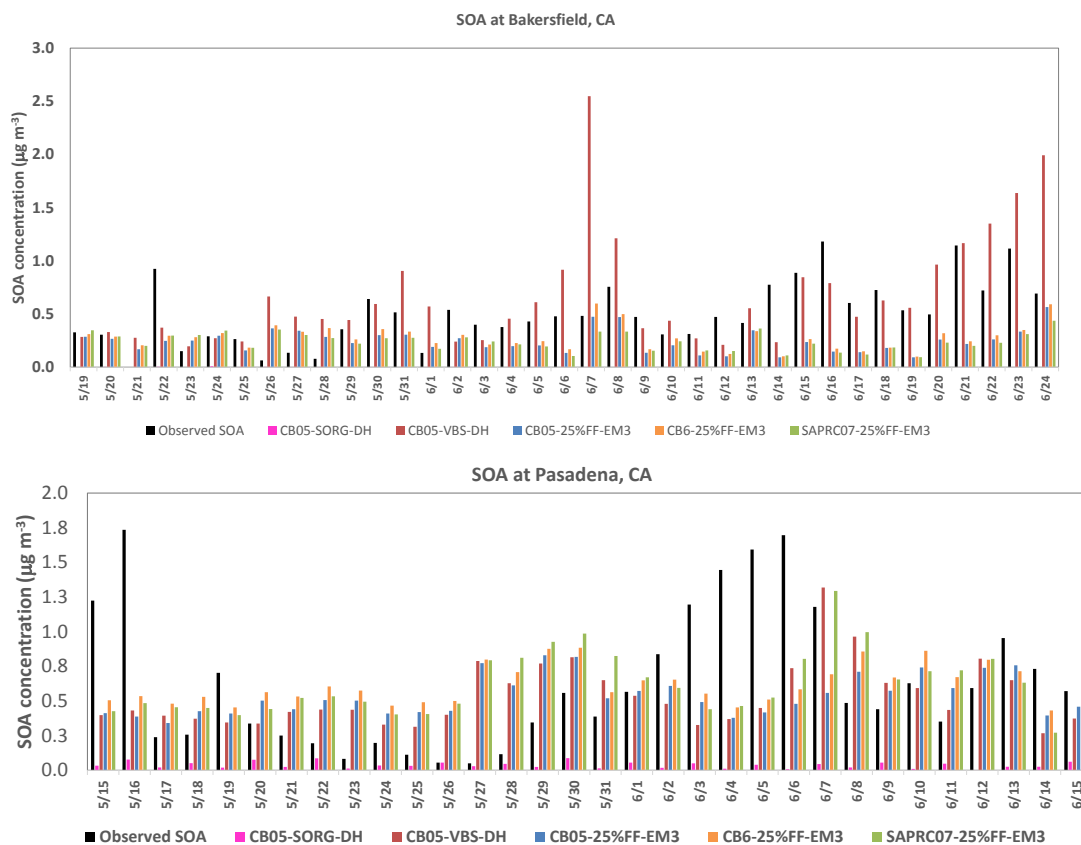


Figure 4. Comparison of obs SOA vs. sim SOA at CalNex sites in Bakersfield and Pasadena in California.

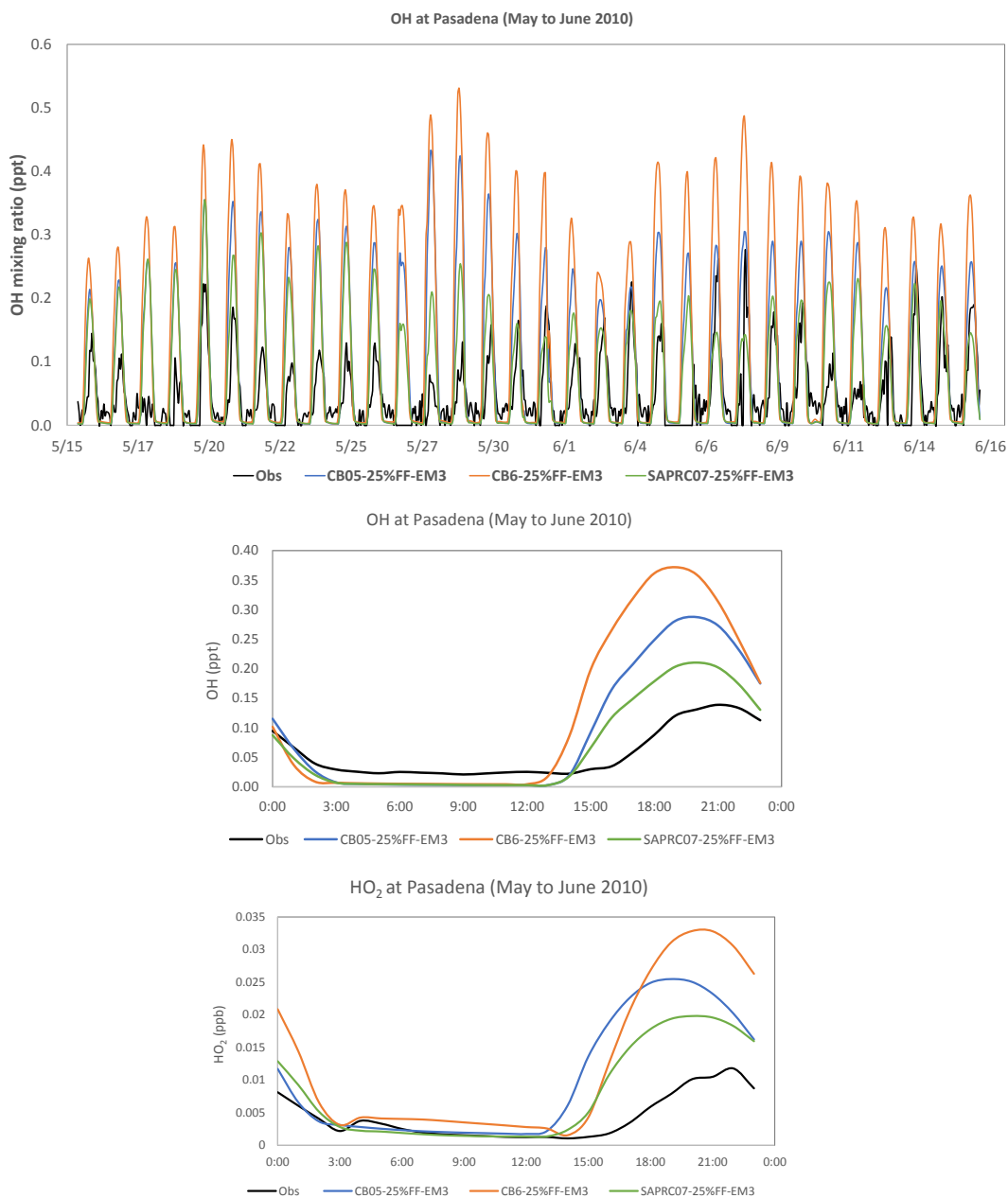


Figure 5. Time series of OH and diurnal plots of OH and HO<sub>2</sub> at Pasadena, CA during CALNEX, 2010.



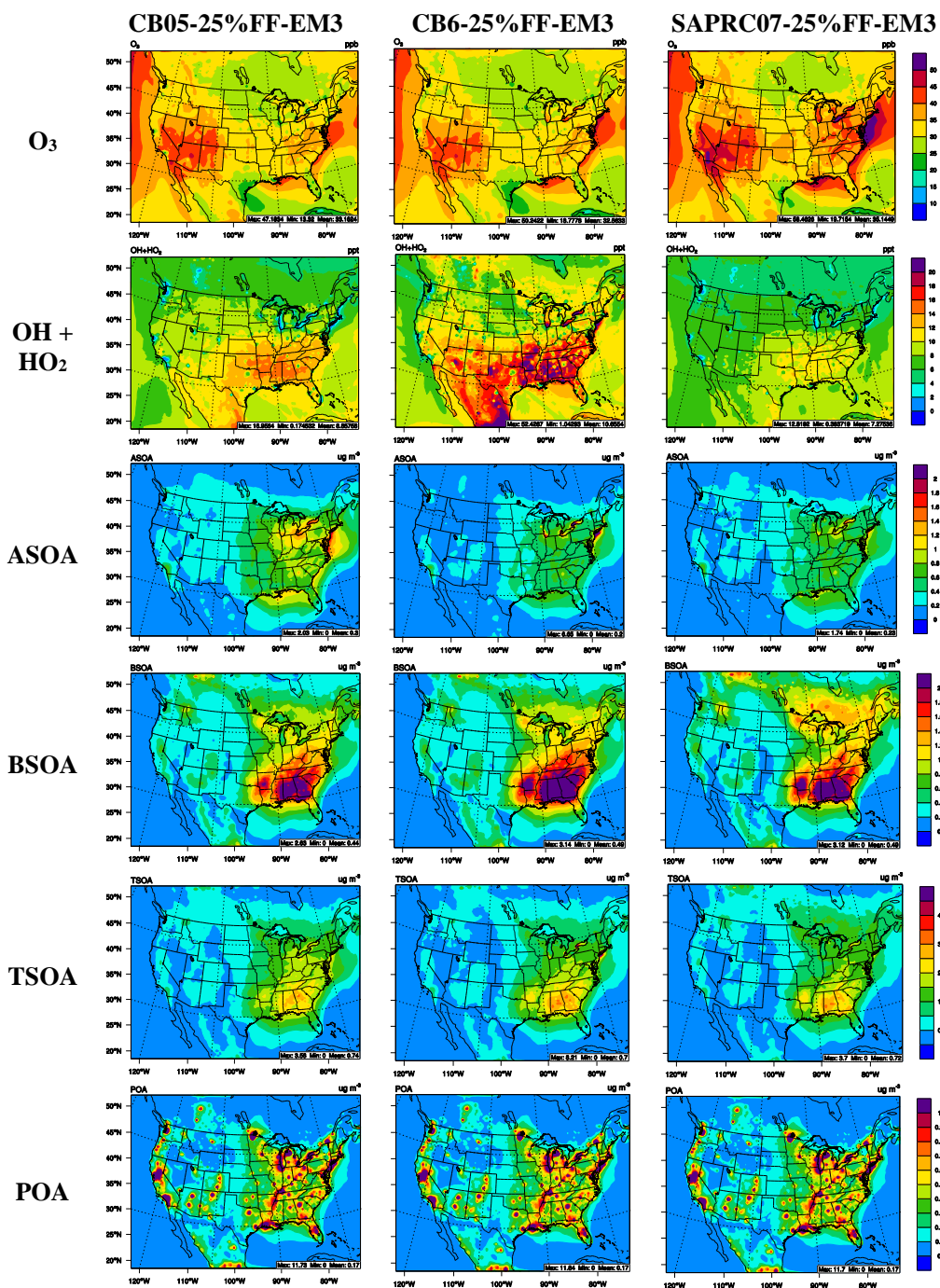


Figure 6. Spatial plots of several gas and aerosol species for the three cases with different gas-phase mechanisms.



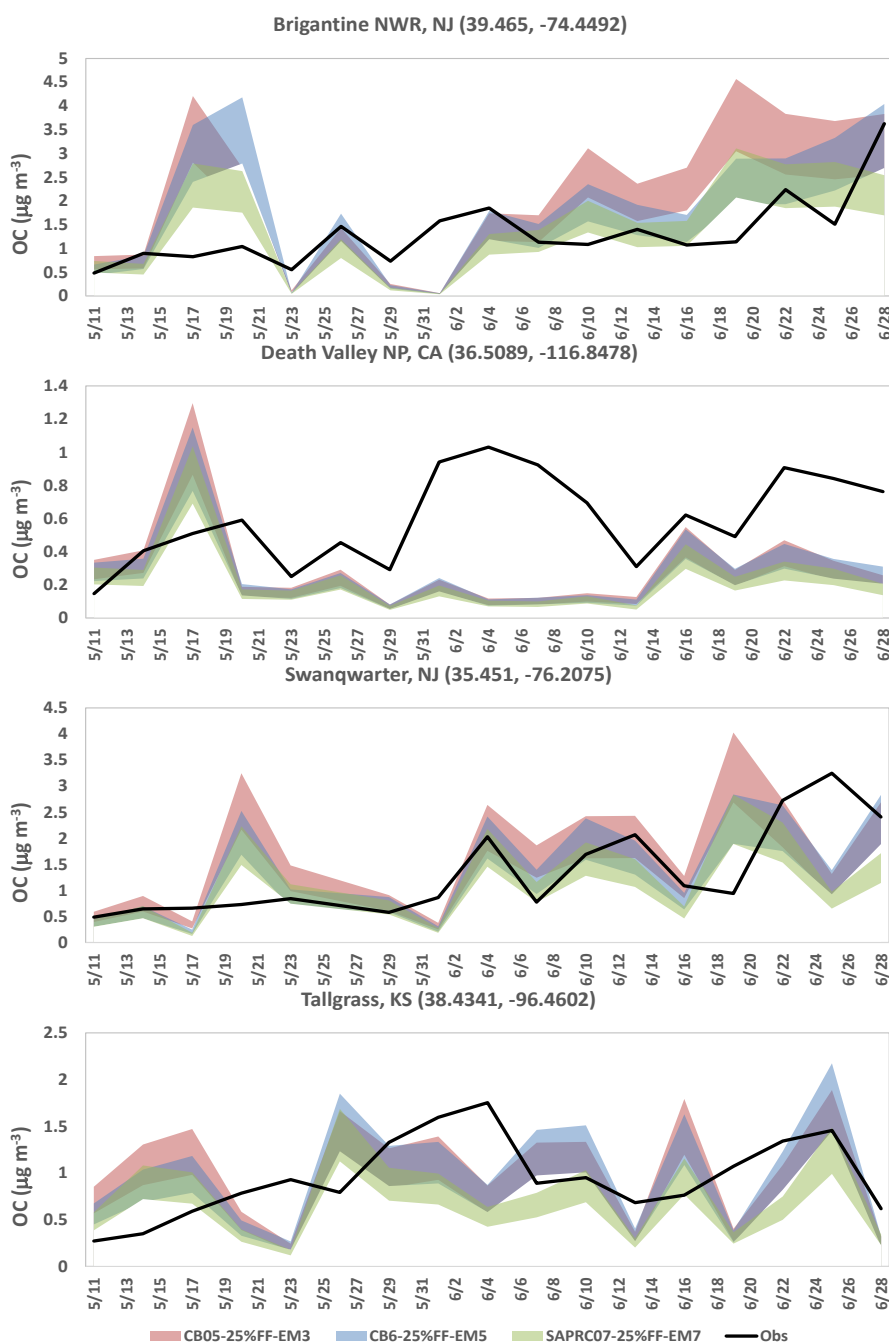


Figure 7. Timeseries plots of IMPROVE OC vs. simulated OC at selected sites from sensitivity simulations of different gas-phase mechanisms. The colored bands represent the range of OC values for ratios 1.4 to 2.1.

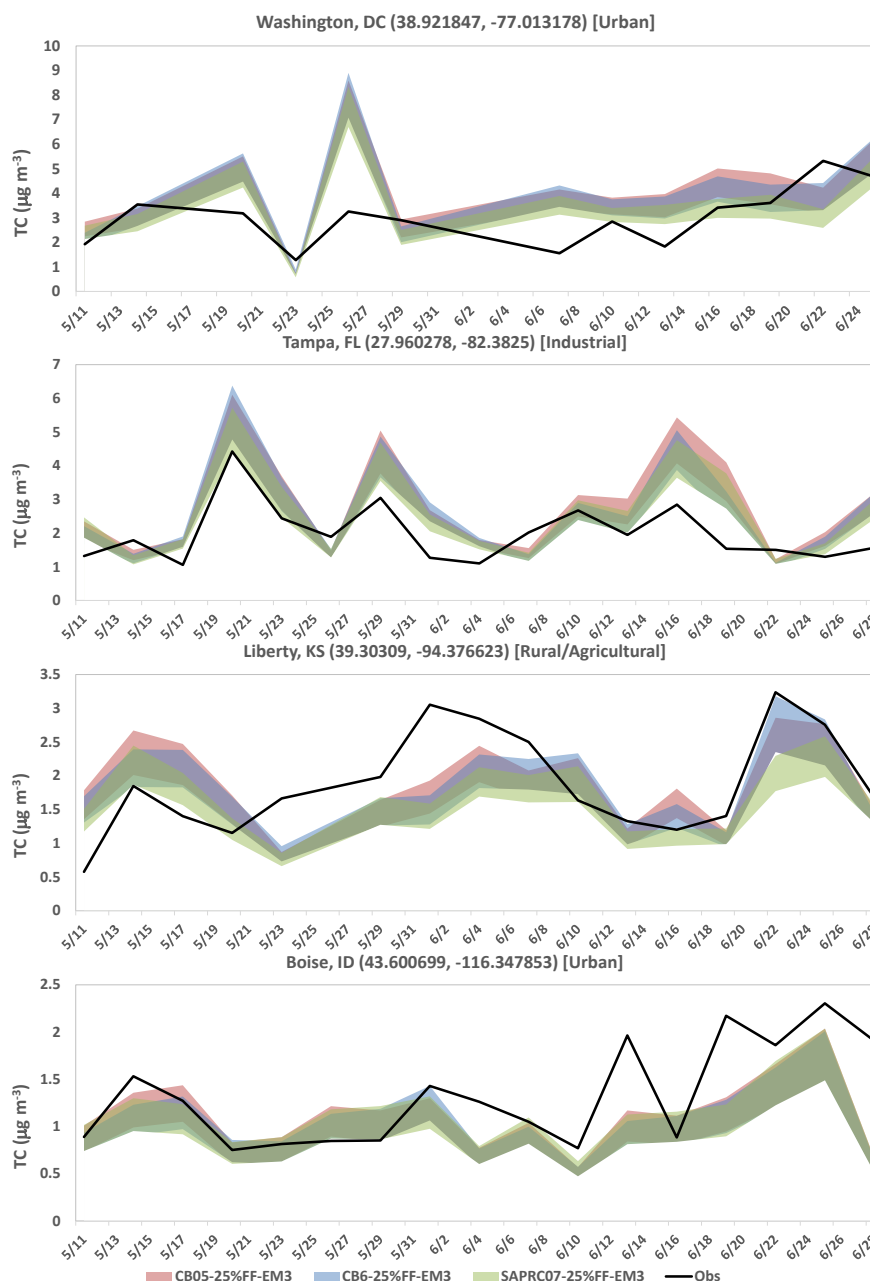


Figure 8. Timeseries plots of STN TC vs. simulated TC at selected sites from sensitivity simulations of different gas-phase mechanisms. The colored bands represent the range of OC values for ratios 1.4 to 2.1.

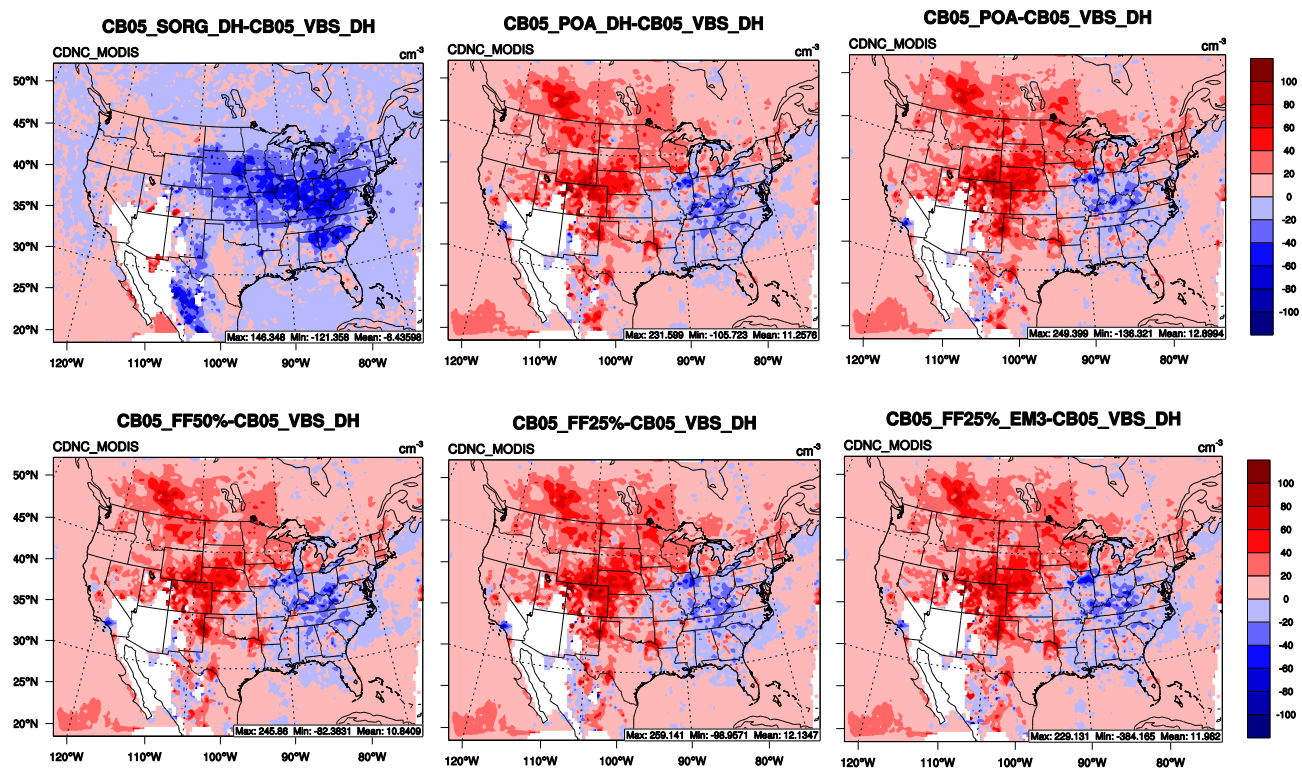


Figure 9. Impact of different VBS case on CDNC in warm clouds. The plots show the differences between the different sensitivity simulations and CB05\_VBS-DH.

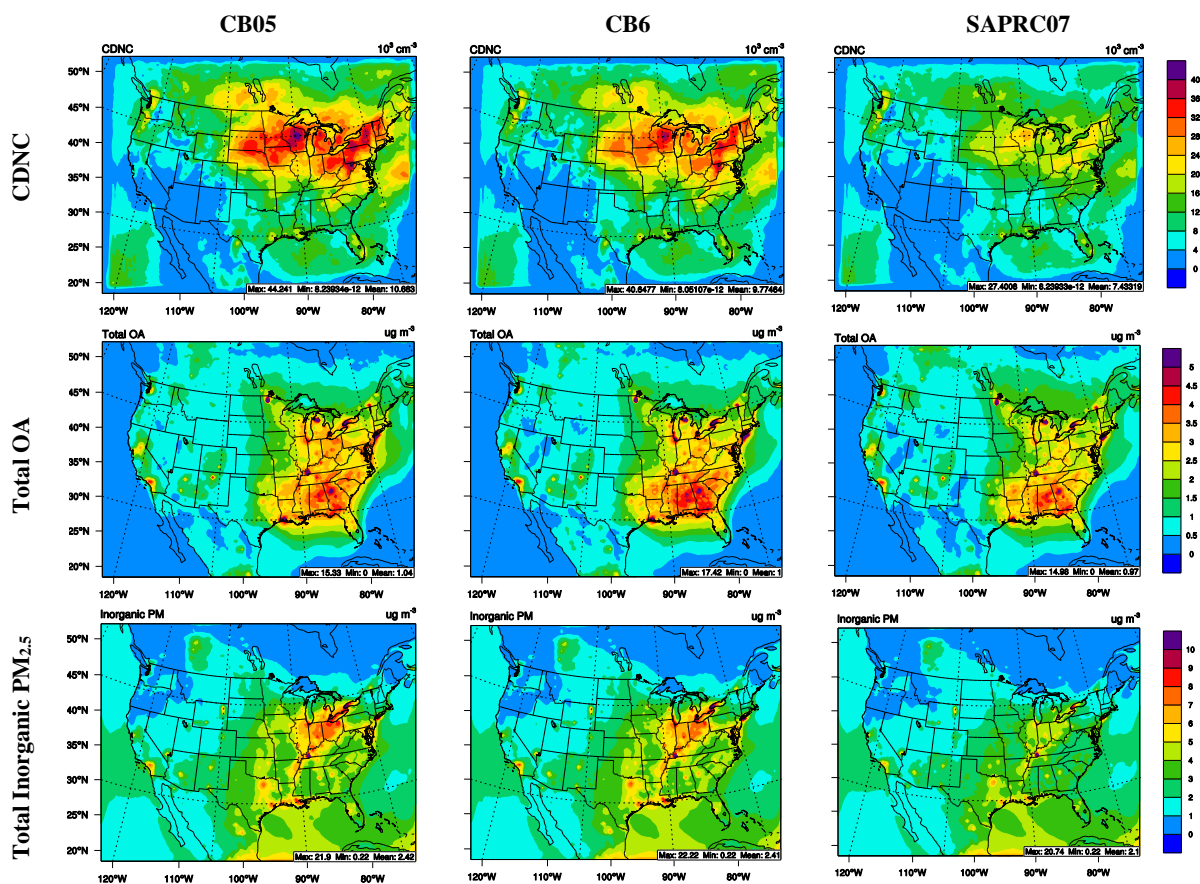


Figure 10. Spatial plots of CDNC, total surface OA and total inorganic PM<sub>2.5</sub> concentrations from different gas-phase mechanisms.

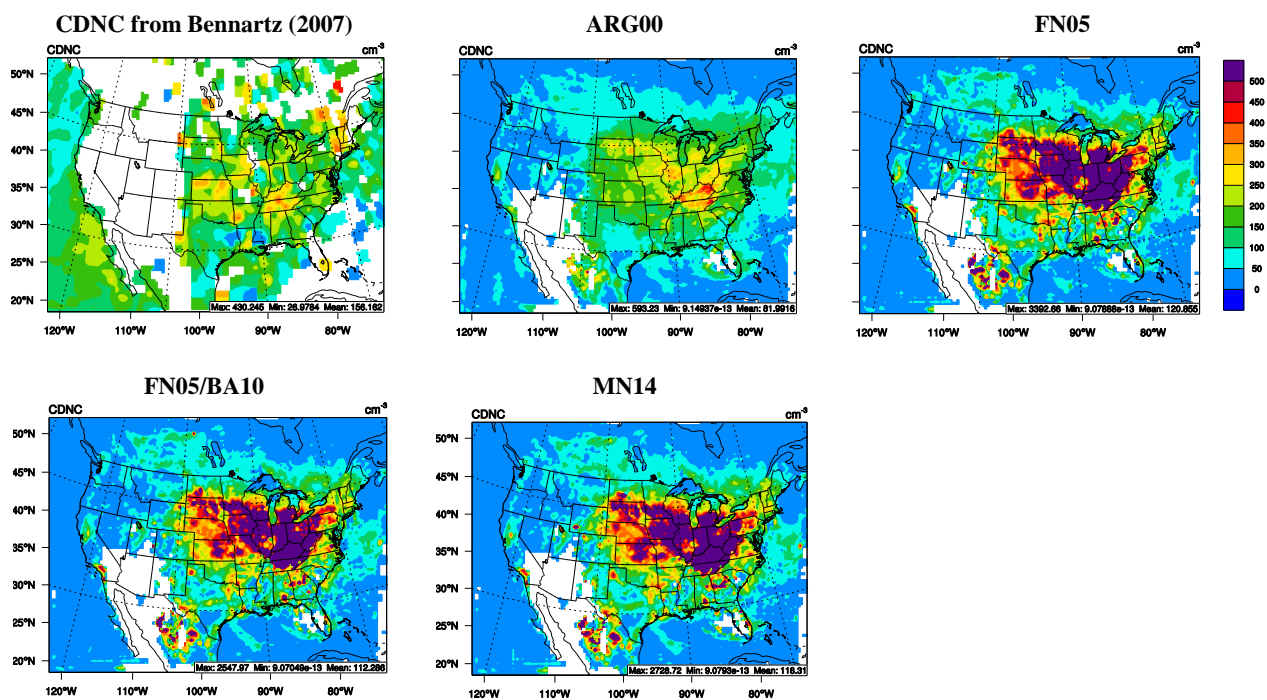


Figure 11. Spatial plots for MODIS-derived CDNC from Bennartz (2007) and simulated CDNC from CB05\_25%FF\_EM3 ARG00, FN series, and MN14 from May to June 2010.

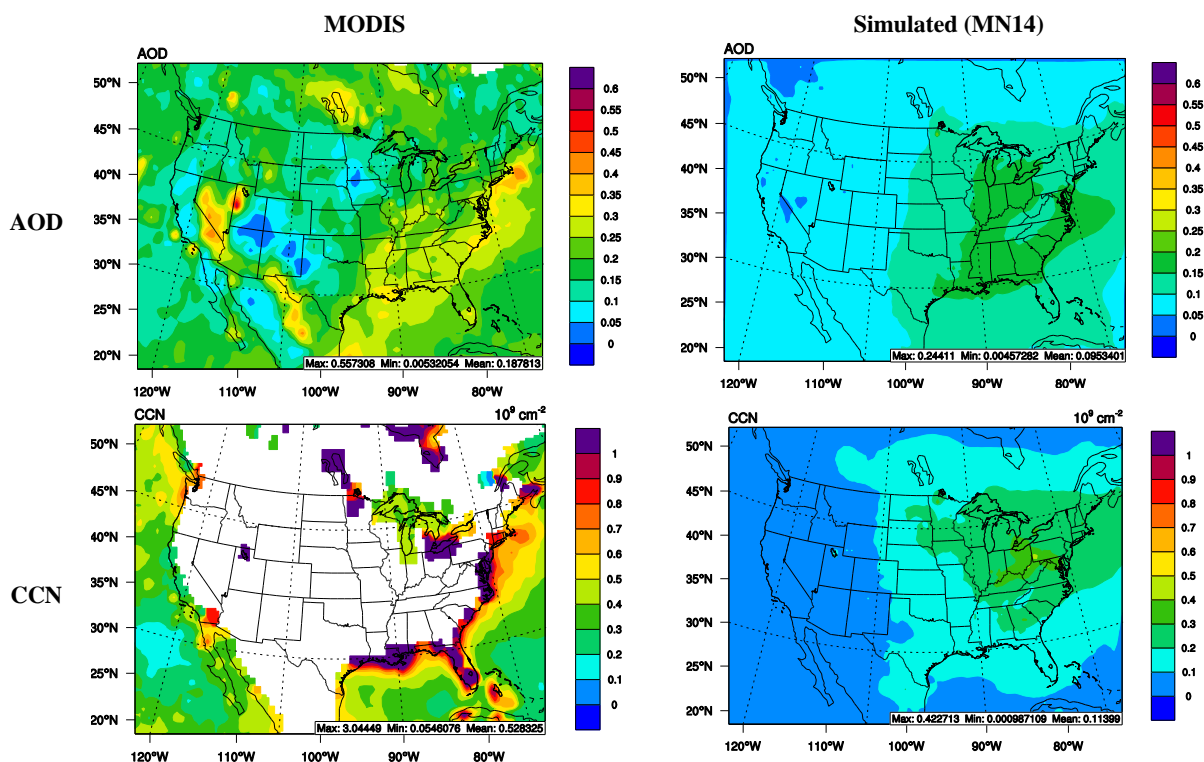


Figure 12. Plots of MODIS AOD and CCN against simulated AOD and CCN from MN14 with CB05\_25%FF\_EM3.